EFFECTIVENESS OF VARIOUS TECHNIQUES IN REDUCING NOISE GENERATED IN MEASURING TORSIONAL VIBRATION

A Thesis

by

AARON MICHAEL SCHOMERUS

Submitted to the Office of Graduate Studies of
Texas A&M University
in partial fulfillment of the requirements for the degree of

MASTER OF SCIENCE

August 2007

Major Subject: Mechanical Engineering

EFFECTIVENESS OF VARIOUS TECHNIQUES IN REDUCING NOISE GENERATED IN MEASURING TORSIONAL VIBRATION

A Thesis

by

AARON MICHAEL SCHOMERUS

Submitted to the Office of Graduate Studies of
Texas A&M University
in partial fulfillment of the requirements for the degree of

MASTER OF SCIENCE

Approved by:

Chair of Committee,	John M. Vance
Committee Members,	Alan B. Palazzolo
	Cesar O. Malave
Head of Department,	Dennis O'Neal

August 2007

Major Subject: Mechanical Engineering

ABSTRACT

Effectiveness of Various Techniques in Reducing Noise
Generated in Measuring Torsional Vibration. (August 2007)
Aaron Michael Schomerus, B.S., Sam Houston State University;
B.S., Texas A&M University
Chair of Advisory Committee: Dr. John M. Vance

Torsional vibration can be characterized as the cyclic variation of shaft speed, which can cause various failures in rotating machines, such as: gear-tooth breakage, blade-off due to blade fatigue in steam turbines, break-off of shafts, and overloading of components fitted onto the shaft. Commercially, there are only a few systems available that measure this type of vibration as compared to lateral vibration measurement systems. Most of these systems required modifications to the rotating machine, which in some cases are unacceptable. Therefore, it has become common practice to develop in-house torsional vibration measurement systems.

A common measurement technique, called Time Interval Measurement (TIMS), calculates the instantaneous speed of the shaft from a frequency modulated carrier wave. Since torsional vibration is the cyclic variation of shaft speed, the shaft speed can be used to determine torsional vibration. Noise can be easily introduced into this type of system masking the torsional vibration; this was apparent in the measurement system developed by Kar, which was used as a baseline for the experiments conducted in this thesis. Various techniques were employed to reduce the effects of the noise in the measurement system, such as (1) created an algorithm, different than the one used by Kar, to calculate shaft speed, (2) increased the sampling rate of the data acquisition boards, (3) resampled the shaft speed into the order domain in order to remove harmonic noise, and (4) created an algorithm that corrects the shaft speed calculation to account for unequal spacing of encoder segments.

These noise reducing techniques were compiled into a LabVIEW™ program in order to develop a robust measurement system. Each technique was tested individually on two test rigs constructed at the Turbomachinery Laboratory. Each technique proved to reduce the noise introduced into the system, but the geometric compensation algorithm proved to be the most effective in reducing the noise. This thesis proved that an in-house measurement system could be developed at a relatively low cost and with relative ease.

DEDICATION

To my loving wife. You are my rock.

ACKNOWLEDGEMENTS

I would like to thank Dr. John M. Vance for the opportunity to work under his guidance and leadership. A special thanks to Preston Johnson and National Instruments for their support in developing the LabVIEW™ code; without their assistance, this thesis would not be possible. I am extremely grateful to my colleagues at the Turbomachinery Laboratory for their assistance through out this project, especially Adam Jones for his expert knowledge with electronics and computers and Vinayaka Rajagopalan for his help in taking measurements and constructing one of the test rigs used.

I would like to thank the Turbomachinery Research Consortium (TRC) for the financial support of this project. Last but not least, I would like to thank my wife, parents, and family for their emotional support and prayers.

TABLE OF CONTENTS

CHAPTER Page

LIST OF FIGURES

FIGURE Page

FIGURE Page

LIST OF TABLES

CHAPTER I
INTRODUCTION

Torsional vibration, in rotating machines, can be defined as the oscillatory motion of a rotor as it rotates. Torsional vibration can also be viewed as the cyclic variation of shaft speed. Torsional vibration, in rotating machines, can cause various failures, such as: gear-tooth breakage, blade-off due to blade fatigue in steam turbines [1], break-off of shafts, and overloading of components fitted onto the shaft [2]. Common sources of torsional vibration include electromagnetic torques from line frequency in electric motors and generators as well as long drive trains with massive inertial components. Torsional vibration can be used as a diagnostic tool to detect sudden changes in blade natural frequencies, which are coupled to the shaft torsional modes, indicating blade cracking as shown in Figure 1 [3].

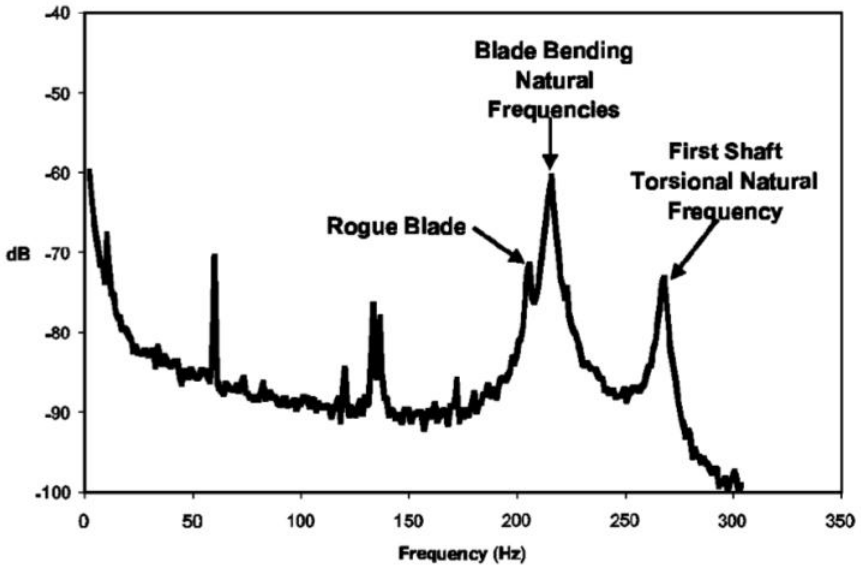

Figure 1: Frequency spectrum displaying a fatigued blade.

This thesis follows the style of the *Journal of Sound and Vibration*.

Measurement Methods

Torsional vibration is not an easy measurement to make as compared to measuring lateral vibrations. Often times, torsional vibration is measured indirectly and then back calculated to obtain the actual torsional displacement. Such measurement methods include frequency modulation, time interval measurement, amplitude modulation, and side-band methods. The oldest and most widely known measurement method uses strain gages to directly measure the amount of twist in the shaft [1].

Strain Gage

In this method, strain gages are bonded to the surface of the shaft and oriented in the directions of principal strain. The electrical resistance of a strain gage is proportional to the mechanical strain of the shaft material. The mechanical strain of the shaft is then related to the amount of twist in the shaft. In order to measure small changes in the resistance due to the strain of the shaft material, strain gages used to form a Wheatstone bridge [1]. A schematic of the Wheatstone bridge is shown in Figure 2 [1].

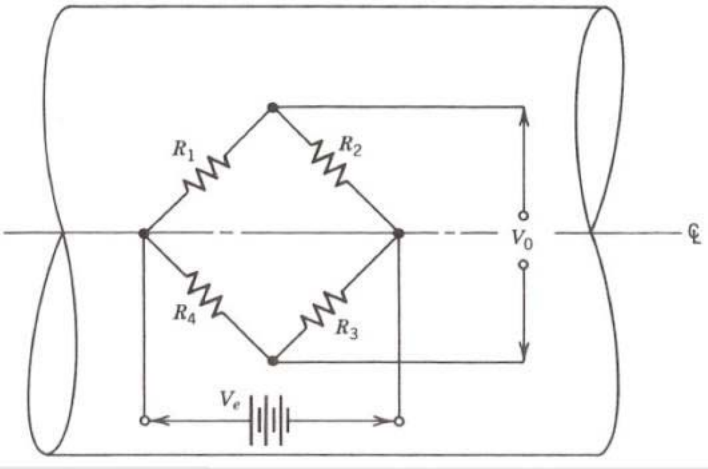

Figure 2: Strain gages bonded to a shaft surface forming a Wheatstone bridge.

This method is extremely accurate if properly installed and calibrated. One major disadvantage is that it requires some modifications to existing machines. A problem that must be addressed is transferring the signal from the rotating shaft to the stationary housing. Slip rings or radio telemetry are common methods for transferring

the signal [1]. The harsh environments that can exist with machines placed in the field often lead to dirty slip ring brushes or radio telemetry interference which can cause errors in obtaining the signal from the shaft.

Frequency Modulation

A less intrusive method in measuring torsional vibration is the frequency modulation method [1]. This method works by first measuring a carrier signal, often times accomplished using a shaft encoder and a non-contacting transducer, such as a magnetic or eddy current proximity probe. As each segment of the encoder passes under the transducer, a pulse is generated creating a pulse train, seen in Figure 3.

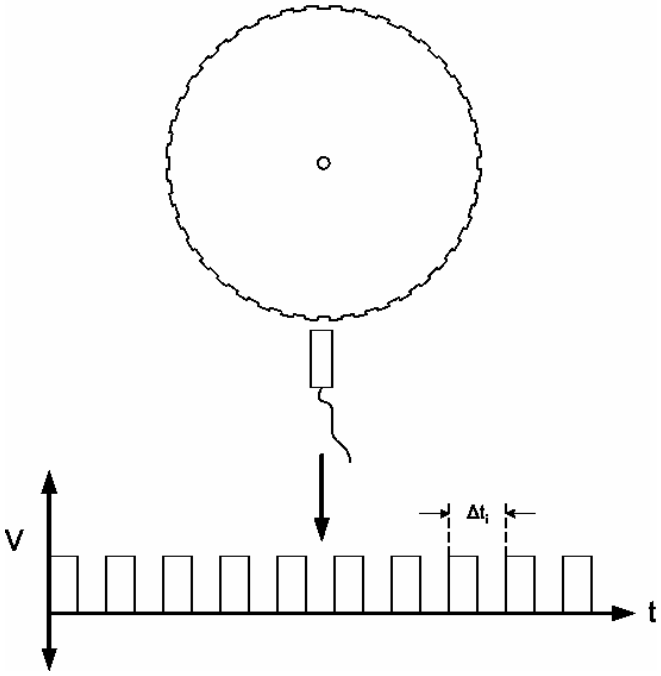

Figure 3: Pulse train created from shaft encoder.

A square wave is not the carrier wave that will be produced directly from the measurement transducer. Often times it resembles a modulated sine wave, but it depends upon the encoder and transducer used. In order to produce the square wave seen in Figure 3, additional electronics are needed.

Since torsional vibration is the cyclic variation of the shaft speed, the torsional frequency will modulate the pulse train created from the encoder segments passing under

the transducer; an example of the frequency modulated pulse train is displayed in Figure 4 [1].

Figure 4: Pulse train modulated by torsional vibration.

For one type of frequency modulation instrumentation, this signal is used to generate an AC signal with its DC amplitude proportional to the instantaneous speed of the shaft and the AC component equal to the torsional vibration velocity [1]. Integrating this signal yields the torsional vibration displacement. The AC signal is generated using electronics that frequency demodulates and conditions the carrier signal. A typical circuit generates a shaped pulse of precision amplitude and width from each pulse, or cycle, of the carrier signal [1]. The resulting square wave from an encoder rotation is integrated to produce a steady DC voltage when the shaft speed is constant [1]. Torsional vibration produces a variation about its mean value.

This accuracy of this method highly depends upon the electronics used to demodulate the carrier signal. A disadvantage to this technique is that noise introduced into the system can generate false frequencies disguising the torsional vibration component.

Amplitude Modulation

Another non-intrusive torsional vibration measurement technique is the amplitude modulation method. Some transducers, like the magnetic probe, produce a carrier signal that will modulate its amplitude as well as its frequency as an encoder segment passes under it. A technique called envelope detection is used to produce a voltage analogous to the torsional vibration velocity [1]; an example of envelope detection is seen in Figure 5.

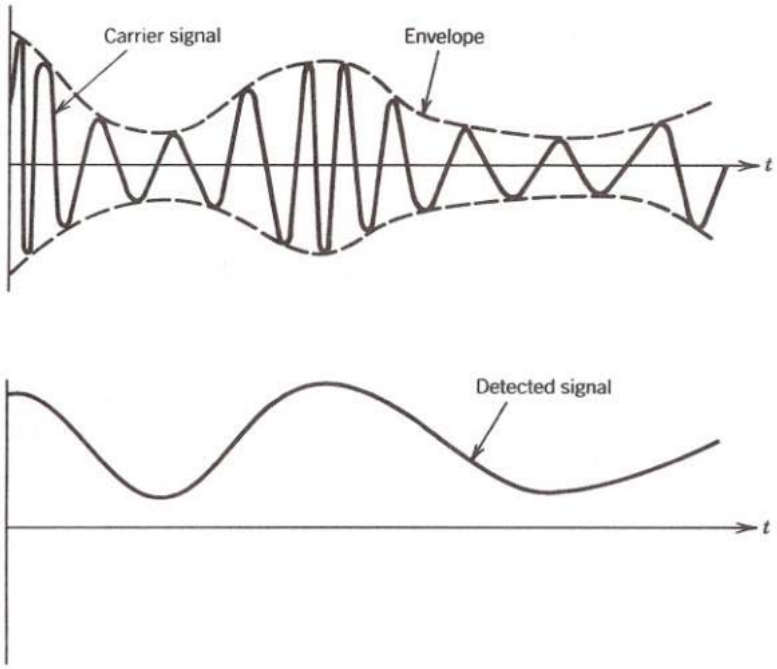

Figure 5: Envelope detection from a carrier wave.

The modulating signal from the carrier wave can then be integrated to give the torsional vibration displacement.

Noise introduced into the system can generate false modulations of the carrier signal making it harder to see the effect of torsional vibration. The accuracy in measuring torsional vibration also depends upon how well the electronics used perform the envelope detection method.

Side-Band

The simplest of the three non-intrusive methods is the side-band method. This measurement technique is performed by taking a FFT of the carrier wave. On the frequency spectrum a prominent peak will appear at a frequency equal to the tooth pass frequency of the encoder. Accompanying this peak to its left and right is a symmetrical array of peaks with decreasing magnitude, called side-bands. This phenomenon is a result of the Fourier series expansion of the frequency modulated waveform [1]. An example of the side-band phenomenon is displayed in Figure 6.

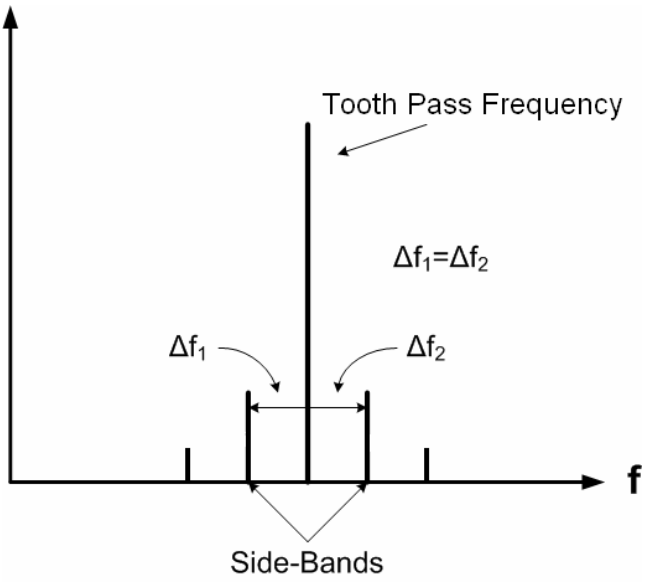

Figure 6: Frequency spectrum displaying side-bands due to torsional vibration.

The torsional vibration frequency is the difference in the tooth pass frequency and the frequency of the closest sideband; in Figure 6, the torsional vibration frequency is equal to Δf_1.

As with the frequency and amplitude modulation method, this method is susceptible to multiple sources of noise. The sources of noise for the side-band method come from measurement and hardware errors that manifest themselves in the acquired carrier signal. Kar in [4] demonstrated in Figure 7 that this method works, but shows how noise can mask the side-bands.

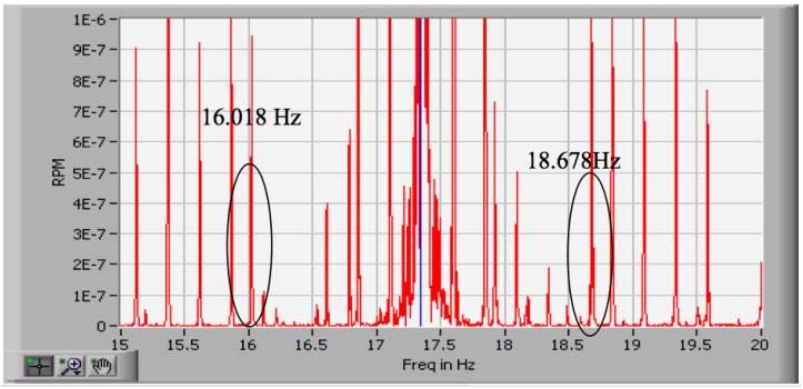

Figure 7: Frequency spectrum of a rotating tumble mill showing side-bands.

This frequency spectrum was taken from the carrier signal of a scaled model of a rotating tumble mill. The peak at 17.3 Hz is the tooth pass frequency and the two peaks circled are side-bands resulting from torsional vibration. The torsional vibration frequency was known ahead of time so the side-band peaks were easily be identified. If the torsional frequency was not known beforehand, identifying the side-bands would prove much more difficult.

Time Interval Measurement System (TIMS)

The TIMS method is another non-intrusive measurement technique used to compute torsional vibration in a system. The method uses the same carrier signal generated in Figure 3. Measuring the time between each pulse and inverting it, the passing frequency of the encoder segments is determined. The instantaneous speed of the shaft can then be calculated by dividing the tooth passing frequency by the number of encoder segments. The fluctuation of the shaft speed (torsional vibration) is observed by taking a Fast-Fourier Transform (FFT) of the instantaneous shaft speed signal generated.

This method is very attractive due to its simplicity and minimal hardware needed to take the measurement. This method is susceptible to a large a amount of noise generated in the system due to measurement and hardware errors that can often mask the torsional vibration component.

Literature Review

French in [5] developed and evaluated measurement techniques for field measurement of torsional vibration. The techniques tested were frequency modulation, amplitude modulation, and side-band analysis method. Strain gages were used as a baseline to which all the other methods were compared to. Testing was done on a laboratory test rig that consisted of a horizontal, slender shaft with two large, inertial disks attached to it. Torsional vibration was exited in the system using a function generator in tandem with a DC motor. Testing was performed under steady-state as well as transient operating conditions. Results showed that all three methods were accurate in

measuring the torsional vibration frequency, but the frequency modulation method was the best at measuring the amplitude of the torsional vibration.

Vance in [1] described a Time Interval Measurement System (TIMS) which utilizes a digital circuit for a tachometer in order to measure torsional vibration. A black and white striped tape, called 'zebra' tape, was used as an encoder. A fiber optic transducer produced a square wave which turned 10 MHz counters on and off recording the passing times of each line of the tape. A computer was used to invert the passing times producing angular speed versus time. Uneven spacing of the lines of the encoder was identified as a source of noise for the system. It was overcome by recording the noise at a constant speed with no torsional vibration and subtracting it out of the system later. Experimentation of the TIMS method was performed on a vertical torsional vibration test rig used for experiments in this thesis.

Fu and Yan in [6] used a digital measurement system similar to Vance in [1] to measure torsional vibration on a test rig that consisted of 4 inertial disks mounted on a slender shaft. A technique was developed that was used to correct for geometric imperfections in the encoder. The technique used a reference signal to trigger a high frequency counter which measured the pulse position of each passing encoder segment. The pulse train of the encoder was recorded at a constant running speed with no torsional vibration. Next the pulse train was recorded while the system was excited by torsional vibration. The pulse position of each encoder segment under the different operating conditions was compared in order to determine the phase shift between the two; torsional vibration was determined from the phase shift. This method was accurate in measuring torsional vibration under steady-state operating conditions.

Williams in [7] compared using analog and digital tachometers. The technique used was similar to Vance's method for torsional vibration calculation. All of his testing was done through simulations only. He identifies the following as sources of error in digital measurements: (1) aliasing, (2) measuring tooth-pass time, (3) demodulation process, (4) tooth spacing variation, (5) magnetic pickup movement. He discussed certain methods to minimize these errors such as increasing the sampling rate,

windowing the data, increasing the number of encoder segments, and balancing the system. He proposed that digitization of a magnetic pickup signal with a high-bit A/D converter would reduce the errors that accompanied a digital tachometer in measuring tooth pass times.

Gomez de Leon et al. in [8] presented a low-cost method for measuring torsional vibration. The method for measuring torsional vibration was to purposely place a reference in the encoder used to measure the angular velocity. An example of such a reference point would be the end-effect created when wrapping the zebra tape around a shaft. The black or white line created at this end point was obviously be much wider than the others and could be identified easily in the pulse train. This pulse was used to identify the other pulses. An algorithm was developed for each individual encoder segment in order to calculate the angular velocity of each segment. Measurements were performed on a rotating test rig with a double cardon joint. The change in instantaneous speed was calculated at both ends of the joint and compared to one another in order to observe the torsional vibration occurring within the joint.

Maynard and Trethewey in [3] and [9] designed a measurement system in order to measure blade and shaft torsional natural frequencies. The measurement system uses a zebra tape encoder and a digital tachometer; the method for calculating torsional vibration was similar to what Vance uses in [1]. A test rig with rods used to model turbine blades was used in testing the measurement system. Maynard demonstrated in the frequency spectrum of the instantaneous speed that 'skirts' can be seen with the harmonics of the shaft running speed. These 'skirts' can sometimes mask important frequency components if they occur around a harmonic. The time-series data was resampled into the order domain in order to remove the order components; it is then resampled back into the time-series domain and a series of averages was taken. This method proved to reduce the 'skirts' of harmonics dramatically revealing hidden frequencies that were close to the harmonics.

Resor in [10] and [11] continued the research done by Maynard and Trethewey. He presented a method for compensating for the difference in encoder segment length.

The method involves calculating the passage time of each encoder segment at a constant speed with no torsional vibration. A ratio is developed between each encoder passage time and the time required for one revolution. Averaging was performed over many revolutions and a correction factor was developed; this correction factor was applied to each time interval. Also, a new resampling technique for the time-series data was employed that used a cubic spline to convert the non-constant time intervals due to changes in speed to constant time intervals.

Background Research

Kar in [4] developed a torsional vibration measurement system in LabVIEW™ to measure torsional vibration created from the oscillatory motion of grinding medium in a tumble mill [12]. The measurement method used was derived from the TIMS method. The model test rig, which measurements were taken from, is seen in Figure 8 [12].

Figure 8: Tumble mill test rig.

A galvanized chain wrapped around the circumference of the drum, seen in Figure 9 [12], was used as an encoder index to excite a magnetic transducer.

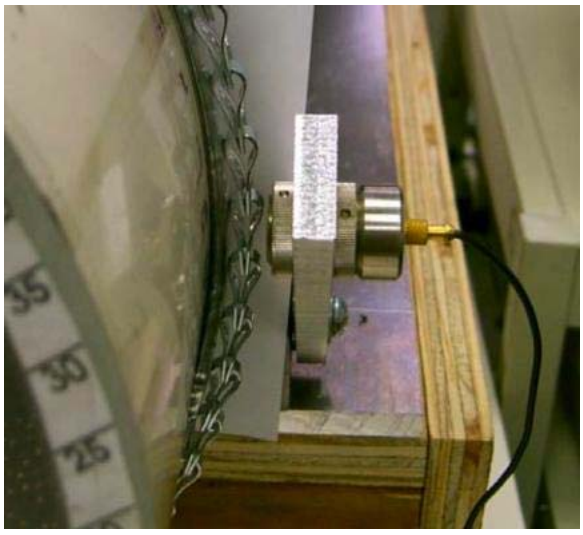

Figure 9: Galvanized chain with magnetic probe.

A pulsating signal was created from the links of the chain passing over the magnetic probe. The instantaneous speed of the rig was found by counting the number pulses in a given time period and using the following algorithm.

$$\omega = \frac{N_T}{N_E} \cdot 60 \ \left(rpm\right) \tag{1}$$

where N_T is the number of pulses in a given time period and N_E is the total number of links in the chain. A plot of the instantaneous speed is displayed in Figure 10 [4].

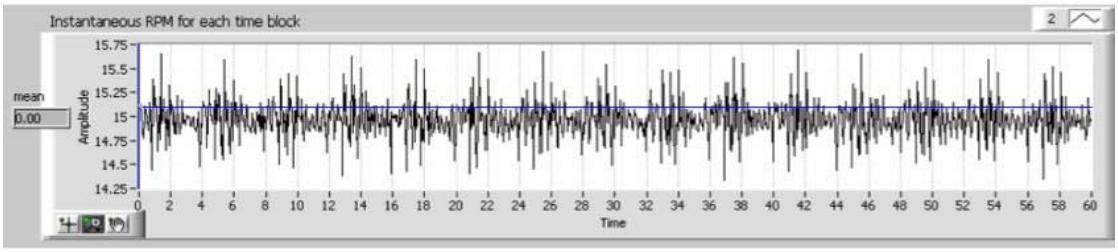

Figure 10: Instantaneous speed of tumble mill.

The average speed of the tumble was calculated to be 15 rpm.

A FFT was taken of the time-series plot in Figure 10 in order to view the speed modulating frequency (torsional vibration). The FFT of the plot in Figure 10 is displayed in Figure 11 [4].

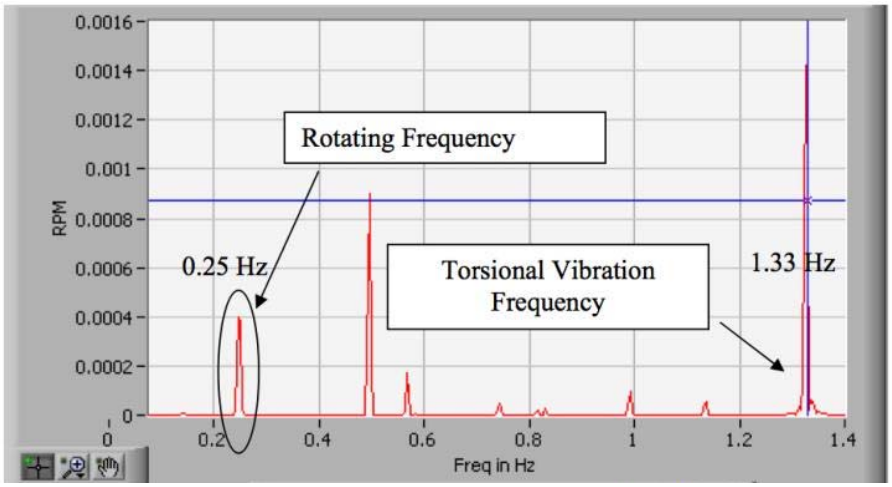

Figure 11: FFT of instantaneous speed of the tumble mill.

This torsional vibration measurement system is very attractive due to its simplicity in acquiring the frequency modulated signal as well as calculating the instantaneous speed of the tumble mill. The measurement system was relatively cheap, as compared to similar measurement systems, due to the use of a low-cost data acquisition device available through National Instruments and the use of a galvanized chain as an encoder.

The torsional vibration frequency was first determined by counting the oscillations of the grinding medium seen through the Plexiglas cover in a given time period. Knowing the oscillation frequency, the torsional vibration was determined from the multiple peaks observed in the frequency spectrum displayed in Figure 11. For other machines, the torsional vibration frequency is not always known and accompanying noise can make it difficult to determine the torsion vibration frequency.

The appearance of multiple peaks in the FFT of Figure 11 was a result of the 'noisy' signal produced in the graph of Figure 10. Possible sources of noise introduced into the system were the following:

1. A low sampling rate used to count the peaks produced by the passing of each encoder segment in a given time period. The maximum sampling rate of the data acquisition board used in [12] was 100 KHz where most sampling rates used in other measurement systems range from 10-200 MHz. Sampling the modulated

signal coming from the transducer at a low rate runs the risk of missing pulses used to calculate the instantaneous speed.

2. The algorithm used to calculate the instantaneous speed of the tumble mill. The algorithm counts the number of pulses that passes the transducer in a given time period. If the probe is between encoder segments at the end of the allotted time, an error in the calculation of the speed is generated.
3. Changes in speed during a time block of data. The algorithm in the program assumes that the speed was constant during the duration of a time block. Since the modulated signal was sampled at a constant rate, changes in speed during the time block will cause some frequencies in the frequency spectrum to smear covering up possible important information.
4. Encoder used for the test rig. Another assumption used in the instantaneous speed calculation is that the encoder used has equally spaced segments. Using an encoder like a galvanized chain, which can be found at any hardware store, runs the risk that each link in the chain is not equal to the next. Having an encoder with unequal segments will produce an error in the calculation of the instantaneous speed.

All possible reasons given will appear as modulating frequencies of the carrier signal, when in fact they are simply noise. Some errors will appear as harmonics of the running speed of the system.

Research Justification

Commercially, there are only a few measurements systems available that measure this type of vibration as compared to lateral vibration measurement systems. Most of these systems required modifications to the rotating machine, which in some cases are unacceptable. Therefore, it has become common practice to develop in-house torsional vibration measurement systems [1]. Most measurement systems use the methods presented in the Measurement Method sections or a variation of them. The most common method for measuring torsional vibration found through the author's research is the TIMS method. The main reasons for using this method include: (1) non-

intrusiveness in acquiring the modulated carrier signal, (2) relative simplistic algorithm used to calculate the instantaneous speed of the shaft, (3) minimal hardware needed to perform the required measurements, (4) minimal sources of error in performing the technique as compared to the other non-intrusive measurement methods.

In order to minimize the noise introduced into the system, most measurement systems require advanced, high precision equipment such as: (1) high frequency counter/timer boards that can sample a signal in the range of 10-200 MHz, (2) high precision shaft encoders that have extremely high tolerances with many encoder segments, (3) high frequency, non-contacting measurement transducers, (4) advance signal processing equipment that allows for quick and accurate post-processing of the data. All of these things add up to high cost while only reducing some but not all of the noise in the system.

The purpose of this research was to develop various methods that will greatly reduce or eliminate sources of error in measuring torsional vibration while reducing the overall cost of a torsional vibration measurement system. LabVIEW™ by National Instruments is a graphical programming software that allows for quick and easy ways to post-process data that is not available in most signal processing equipment. Using LabVIEW™ in tandem with National Instruments' numerous data acquisition (DAQ) devices can greatly reduce the cost of a data acquisition system. It is also desirable to use of 'make-shift' encoders, like the galvanized chain used for the tumble mill, which can produce an adequate pulse train, eliminating the use of a high cost, precision encoder.

Research Objectives

The main objective of this research was to develop and test different error reducing techniques in order to eliminate the noise generated in measuring torsional vibration using the TIMS method. The following is a list of the techniques developed and/or tested in this thesis:

- created a different algorithm for calculating the angular velocity from the one used by Kar in [4].

- increased the sampling rate of the measurement system
- resampled the time-series signal of shaft speed to an even-angle signal in order to identify and remove harmonic components of shaft speed from the signal.
- developed a method which corrected the algorithm used to calculate the instantaneous speed in order to account for non-equally spaced encoder segments

Each technique proposed was tested individually in order to view their effectiveness in reducing noise. The various techniques were tested together in order to develop a cheap but robust torsional vibration measurement system in LabVIEW™ that reduces the most amount of noise while increasing the accuracy in measuring torsional vibration.

CHAPTER II
METHODOLOGY

As stated in the Research Justification section, it was the purpose of this thesis to develop and/or test various techniques to reduce the noise generated in using the TIMS method for calculating torsional vibration. The baseline for comparing the effectiveness of each technique was the measurement system developed by Kar in [4] explained in the Background Research section. The techniques addressed in this thesis include: (1) changing the algorithm for calculating the instantaneous speed of the shaft encoder, (2) increasing the sampling rate, (3) resampling into the order domain and removing the orders, (4) correcting geometric imperfections in the encoder.

Speed Calculation

The calculation method, used by Kar in [4], for the instantaneous speed of the shaft is displayed in Equation 1. In summary, the speed is found by counting the number of pulses in a given time period and dividing it by the number of encoder segments. The main issue with this method is risking the chance of being between pulses at the end of the time period as seen in Figure 12.

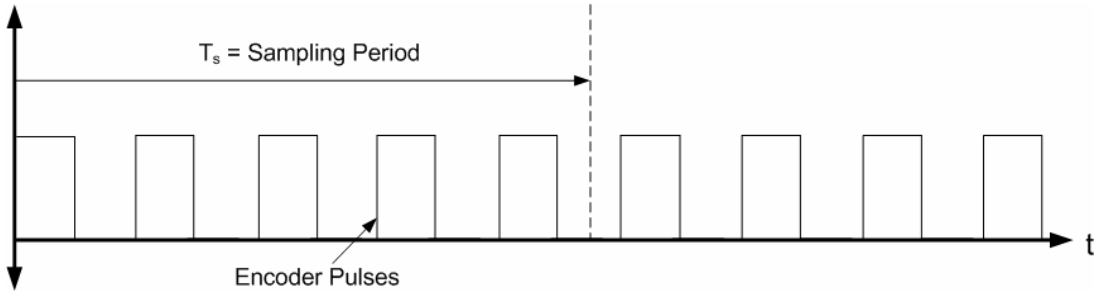

Figure 12: Error in using speed calculation of Equation 1.

This situation causes the calculation of the shaft speed to be less than the actual speed of the shaft creating an apparent fluctuation in the shaft speed that does not really exist. This type of fluctuation in shaft speed can be mistaken for torsional vibration. The error

is reduced by increasing the number of encoder segments, but the best way to eliminate the error is to change the speed calculation method all together.

A more accurate way to measure the instantaneous speed of the shaft is to first measure the pulse position of each encoder segment:

$$\text{Pulse Position} = t(jN + n) \tag{2}$$

where j is the revolution index, N is the number of encoder segments in one revolution, and n is pulse index in one revolution. Next, the pulse width is found by taking the time difference between each pulse position. The pulse width of each encoder segment is used to calculate the instantaneous shaft speed at each segment using the following:

$$\omega\left(jN + n\right) = \frac{1}{t\left(jN + (n+1)\right) - t\left(jN + n\right)} \cdot \frac{60}{N},\ n = 0,1,2,...,N-1 \tag{3}$$

where $\omega(jN+n)$ is in units of revolutions per minute (rpm). The assumptions made for this equation is that the encoder has N equally spaced encoder segments. A time-series signal is generated using the calculated shaft speed at each segment and its corresponding pulse position.

Sampling Rate

Most of the theory developed in this section was adapted from Gomez de Leon et al. in [8]. The period of a pulse, T_i, is calculated by the following:

$$T_i = \frac{p}{f_s}\ \left(\text{sec}\right) \tag{4}$$

where f_s is the sampling rate of the DAQ device and p is the number of samples in the duration of one pulse. An example of the calculation method is displayed in Figure 13 [8].

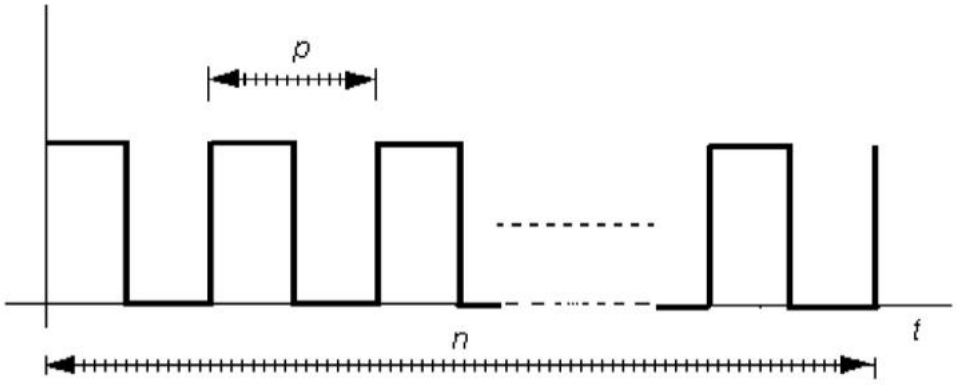

Figure 13: Measuring the time period of one pulse.

An inherent error in measuring the pulse position is due to the fact that the encoder and sample clock in the DAQ board are not synchronized. In an ideal situation, the rise and fall of the encoder pulse train coincides with the sample clock as seen in Figure 14.

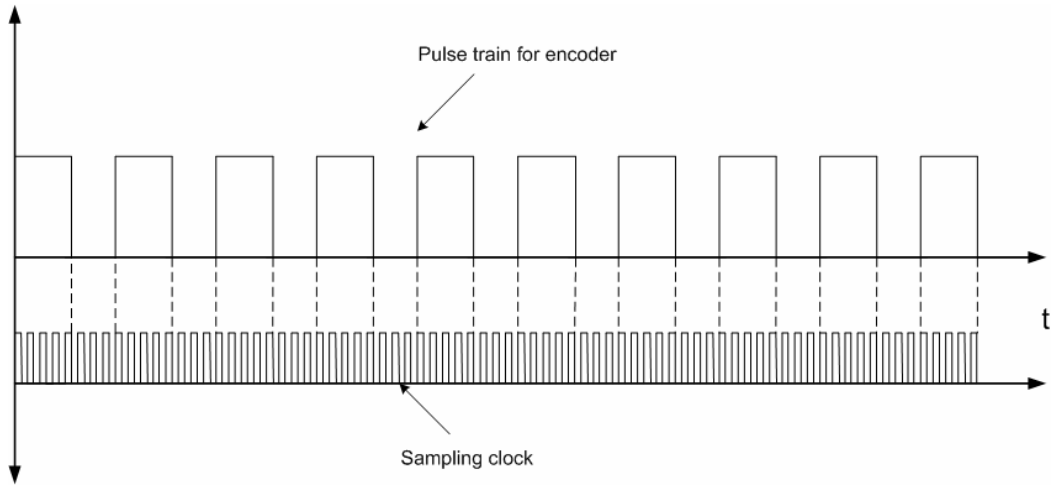

Figure 14: Sample clock synchronized with pulse train of the encoder.

In a real situation, the rise and fall times do not match up, therefore it is impossible to determine the exact duration of a pulse. An error will occur in measuring the start time of one pulse if the sample clock misses the abrupt rise in the pulse's amplitude effectively shortening the duration of the pulse. Likewise, an error will occur at the end of the pulse if the sample clock does not record the abrupt change in the pulse's amplitude effectively lengthening the duration of the pulse. Although the two errors

have opposite effects, it is very unlikely that these errors will cancel each other out. The real time duration for a pulse, t_r, will fall within the following time interval.

$$T_s\left(p-1\right) \le t_r \le T_s\left(p+1\right) \tag{5}$$

where T_s is the sampling period. Putting Equation 5 in terms of the real and measured velocities, ω_r and ω_m respectively, yields the following:

$$-E \le \frac{1}{\omega_r} - \frac{1}{\omega_m} \le +E \tag{6}$$

where

$$E = \frac{m \cdot T_s}{2\pi} \tag{7}$$

The m term in Equation 7 repensents the number of encoder segments in one revolution. It can be stated that the real velocity is related to the measured velocity by the following:

$$\omega_r = \omega_m \pm \Delta\omega \tag{8}$$

where $\Delta\omega$ is the absolute error in the measurement and can be stated as:

$$\Delta\omega \le E \cdot \omega_r \cdot \omega_m \tag{9}$$

This expression can never be evaluated since it is impossible to know the real velocity. Assuming that the least favorable condition is when

$$\omega_r = \omega_m + \Delta\omega\,, \tag{10}$$

then Equation 7 becomes the following:

$$\Delta\omega \le \frac{E \cdot \omega_m^2}{1 - E \cdot \omega_m},\ \forall p > 1 \tag{11}$$

and reducing it using Equations 4 and 7 yields:

$$\Delta\omega \le \frac{\omega_m}{p-1},\ \forall p > 1 \tag{12}$$

This expression determines the maximum methodological error that can occur in the measurement. The error in the measurement becomes smaller as the number of samples in the period of the pulse increases.

The expression for relative error in the measurement can be stated as the following:

$$\frac{\Delta\omega}{\omega_r} \le \frac{1}{p} \tag{13}$$

Combining this equation with Equation 4 yields the following results.

$$f_s = \frac{m \cdot \omega_m}{2\pi \cdot (\Delta\omega/\omega_r)} \tag{14}$$

Assuming:

$$\omega_m = \frac{2\pi \cdot f_s}{m \cdot p} \tag{15}$$

This equation allows for the minimum sampling frequency to be chosen for a given relative error. For example, a machine with 100 encoder segments running at 1800 rpm must be sampled at a rate of 300 KHz in order to ensure a 1% relative error in the measurement. A minimum of 10,000 Samples per time block is required in order to register at least one revolution in the time block.

This analysis shows that an increase in the sampling rate of the data acquisition system greatly reduces the relative error in calculating the duration of a pulse width. Increasing the number of samples per time block will in return increase the number of samples in the period of a pulse resulting in a decrease in the absolute error of the measurement. According to this analysis, these two factors greatly increase the accuracy in calculating the instantaneous speed of the shaft along with measurement of torsional vibration.

Resampling and Order Removal

Measurement errors, such as unequal spacing of encoder segments, manifest themselves as harmonics of the running speed when viewed on a frequency spectrum, making it hard to distinguish between the noise and the torsional vibration. If the torsional vibration occurs near or at the harmonics of the shaft speed, the noise can mask the vibration signal, as in Figure 15 [3].

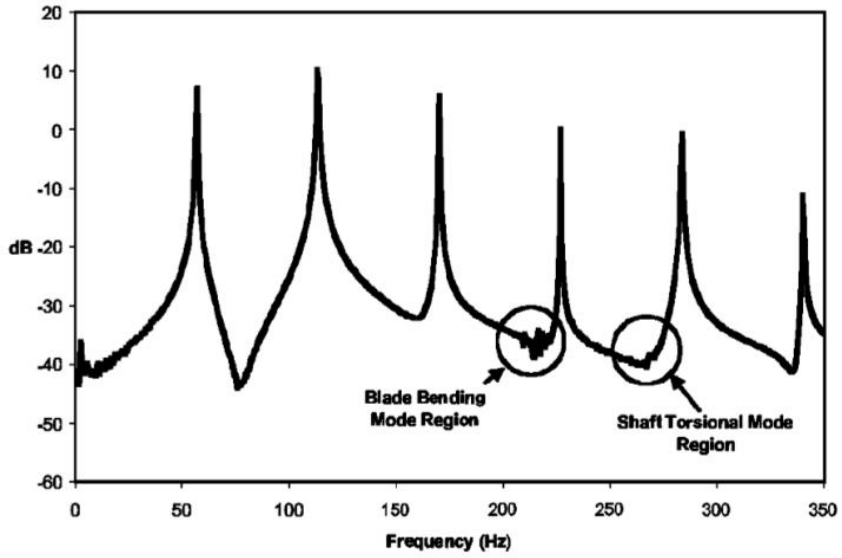

Figure 15: Frequency spectrum with noise masking torsional vibration.

Because most of the noise occurs at harmonics of the shaft speed, resampling the instantaneous shaft speed signal into the order domain can help identify the noise within the array of the signal. Once the harmonics are identified, they can be removed from the signal array revealing important signal components. Removing the harmonics of Figure 15 yielded the results shown in Figure 16 [3].

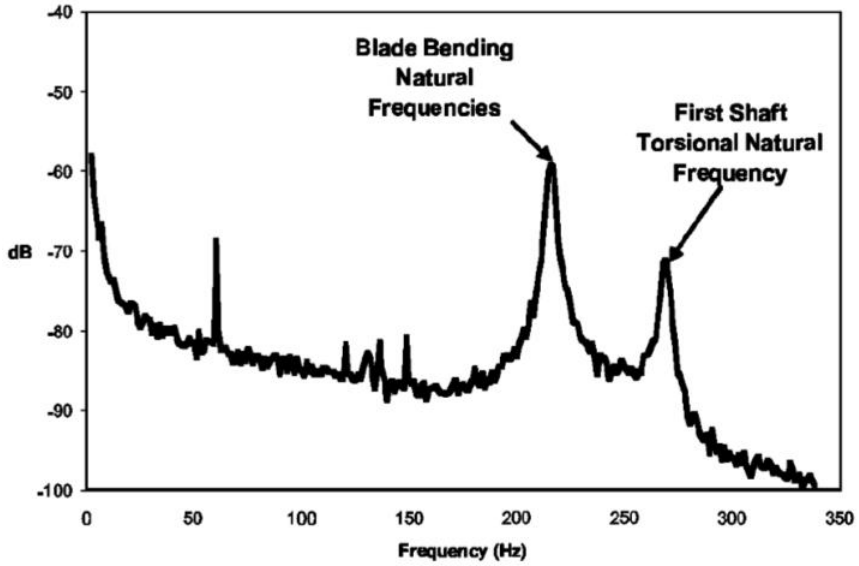

Figure 16: Frequency spectrum with noise at harmonics of shaft speed removed.

The speed profile produced by the process explained in the Speed Calculation section computes the shaft speed at each encoder segment. Resampling into the order domain is performed by creating a speed profile at even-angle intervals which can be viewed as the following:

$$\omega\big(t(jN+n)\big) \Rightarrow \omega\big(\theta(jN+n)\big) \tag{16}$$

The even-angle interval is determined by taking an inverse of the number of encoder segments in one revolution. For a 40 segment encoder, the even-angle interval is 360/40 or 9 degrees. Knowing the angle interval, a signal is generated with the corresponding speed values. Taking an FFT of this signal generates an order spectrum where the harmonics of the shaft speed can be determined from the computed array. The speed values at the harmonics are replaced with a value of zero effectively removing them from the array. Plotting the signal again yields a spectrum with no harmonic components of the shaft speed.

Geometric Imperfection and Compensation

The two methods described in the Speed Calculation section assume that the each encoder segment is equally spaced apart. In reality, all encoders have some error associated in the spacing of each segment, as seen in zebra tape demonstrated in Figure 17 [10].

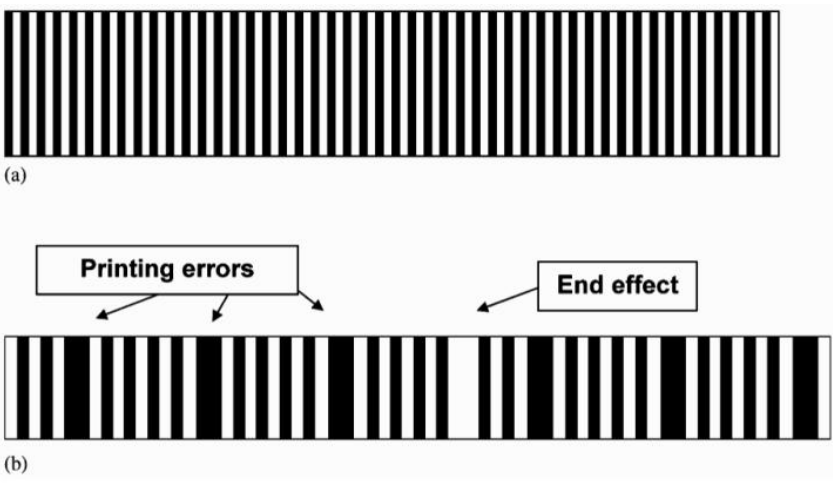

Figure 17: Zebra tape (a) with equally, and (b) unequally spaced lines.

Sources of error in spacing often come from manufacturing inaccuracies and/or improper installation on the machine. For example, errors in zebra tape can come from an end effect created from the first and last stripe resulting in an unequal encoder segment as well as printing errors due to digitization bias error in the printing process [3]. Encoder spacing errors manifest themselves as harmonics of the shaft speed when viewed on the frequency spectrum of the demodulated signal.

One way to decrease these errors is to use a high precision encoder which includes a large number of encoder segments manufactured at extremely high tolerances. High precision usually means high cost, thus a more attractive approach is to use a mathematical process that will geometrically compensate the modulated signal in order to correct the imperfections in the shaft encoder. A diagram of the mathematical process is displayed in Figure 18.

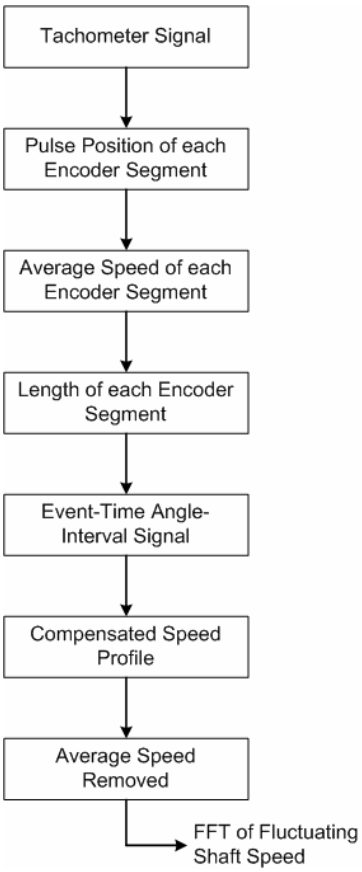

Figure 18: Schematic of geometric compensation process.

The process works by first calculating the average speed at each encoder segment using their corresponding pulse position. The average speed is used to calculate the length (angle) of each encoder segment. Due to the imperfections in the encoder, the angle-interval signal generated occurs at different time intervals. The signal is converted to an even-time signal through spline interpolation. Once the signal has been resampled, the new angle-interval values are used to calculate the instantaneous speed of the shaft and a FFT is taken in order to reveal any fluctuating frequencies in the shaft speed (torsional vibration).

It is helpful to view to the fluctuating shaft speed as a combination of an AC and DC signal as seen in Figure 19.

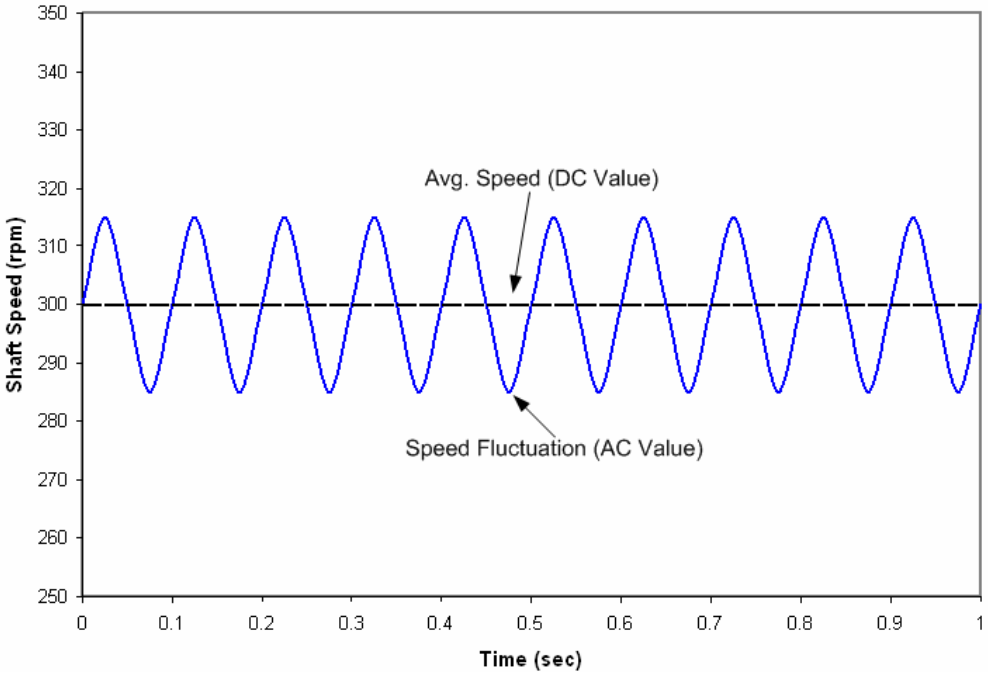

Figure 19: Representation of shaft speed as a combined AC and DC signal.

The DC component of the signal represents the average running speed of the machine. The AC component represents any fluctuation in the running speed whether it is torsional vibration or noise.

Calculation of Average Speed

The first step in the compensation process is to calculate the average speed at each encoder segment. Using Equation 3, the average shaft speed at each encoder segment is calculated over M revolutions by the following:

$$\omega_{avg}(n) = \frac{1}{M}\sum_{j=1}^{M}\frac{1}{t(jN+(n+1))-t(jN+n)}\cdot\frac{60}{N},\ n=0,1,2,...,N-1 \qquad (17)$$

An optimum value for the number of revolutions to use in the average is selected through the process of trial and error until the optimum value is found. A drastic change in speed might occur over the average if many revolutions are used in the average, thereby reducing the accuracy in the average speed calculation.

Computation of the Angle-Interval between Encoder Segments

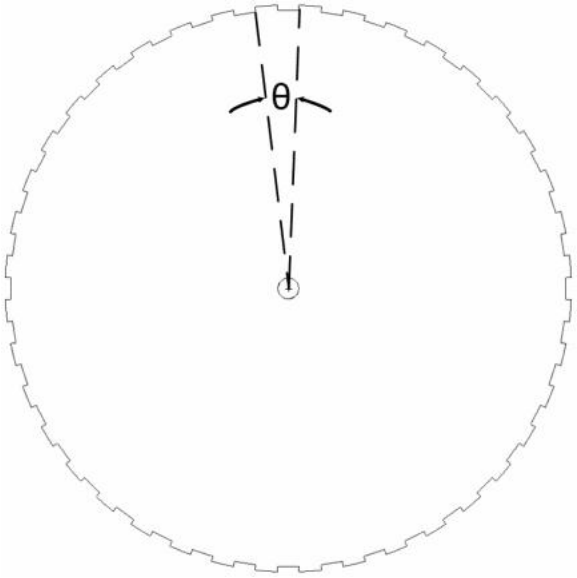

Figure 20: Angle-interval of a 40 segment encoder.

The average speed value was used to calculate the angle-interval of each encoder segment, seen in Figure 20, by multiplying the average speed of each encoder segment by its time-interval:

$$r_j(n) = \omega_{avg}(n)\cdot[t(jN+n+1)-t(jN+n)]\cdot\frac{2\pi}{60} \qquad (18)$$

where $r_j(n)$ is in units of radians (rad). Each calculated angle-interval is averaged over M revolutions:

$$r(n) = \frac{1}{M}\sum_{j=1}^{M} r_j(n), \;\; n = 1,2,...,N \tag{19}$$

Again, an optimum value, through trial and error, is found for the number of revolutions to include in the averaging process. The values of the angle-intervals are used to create a signal similar to that of Figure 21.

Resampling to Even-Time Signal

Variations in the encoder geometry cause the angle-intervals to occur at different times as shown in Figure 21.

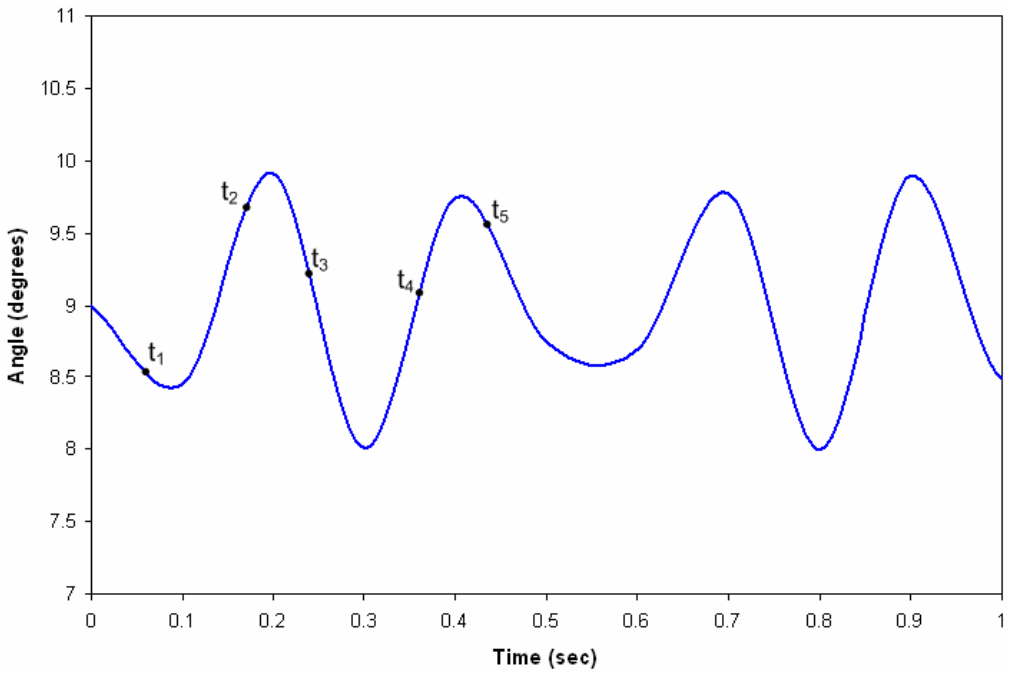

Figure 21: Uneven-time signal

It is common practice to use an FFT to observe the frequency components of the signal. A discrete Fourier transform is based on constant interval sampling, so applying it to an unevenly sampled signal will yield results that are difficult to interpret [10]. Therefore, the uneven-time signal of the angle-interval was interpolated into an even-time angle signal using spline interpolation. Spline interpolation is a function available in

LabVIEW™ which was used for this procedure. The new time-interval for the signal is based on the maximum speed at which the rotor will run:

$$\Delta t = \frac{1}{\omega_{\max} \cdot N},\ \omega_{\max}(\text{rad/sec}) \tag{20}$$

This value determines the maximum frequency that can be observed in the frequency spectrum. Resampling the signal generated in Figure 21 yields the even-time signal displayed in Figure 22 .

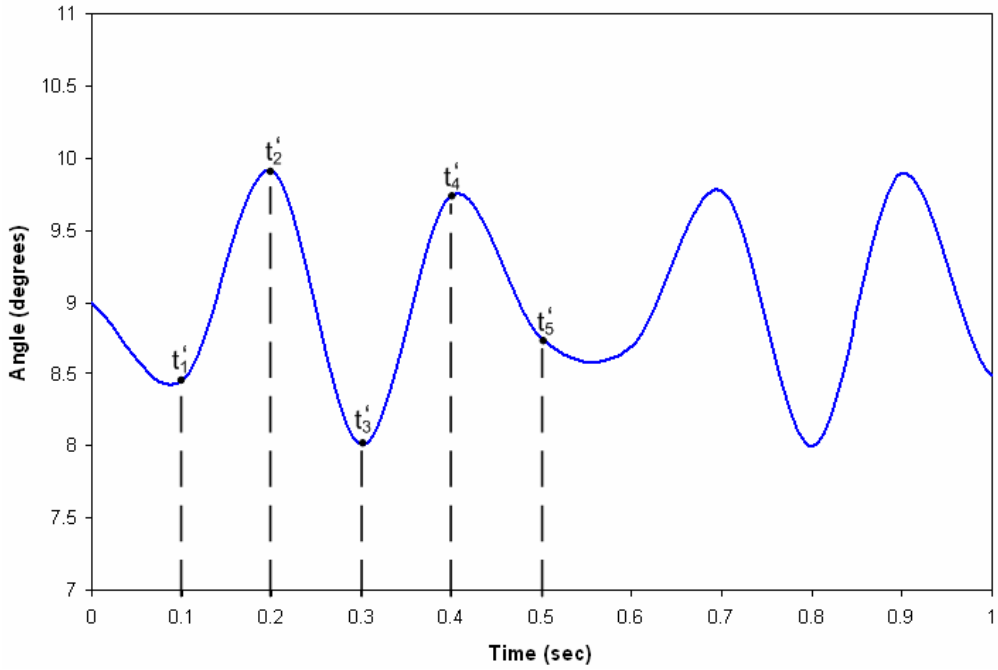

Figure 22: Resampled even-time signal.

Calculation of the Geometrically Corrected Shaft Speed

Using the new angle-intervals and its corresponding time-interval, the speed of each encoder segment, $\omega(t_n)$, is calculated using the following:

$$\omega(t_n) = \frac{\theta(t_{n+1}) - \theta(t_n)}{t_{n+1} - t_n},\ n = 0,1,2,...,N-1 \tag{21}$$

where $\theta(t_n)$ is the resample angle at the resample time index t_n. The time difference is the time interval given in Equation 20:

$$t_{n+1} - t_n = t_n - t_{n-1} = \frac{1}{\omega_{\max} \cdot N} \tag{22}$$

Taking an average of the shaft speed over a specified number of revolutions, the average speed (DC component in Figure 19) is removed from the newly calculated speed signal. A FFT is applied to the shaft speed signal to reveal important frequency components, such as torsional vibration.

CHAPTER III
EXPERIMENTAL TEST RIGS

Two test rigs were used to assess the effectiveness of the measurement techniques presented in the METHODOLOGY in reducing the noise generated in the frequency modulated, carrier signal.

Description of the Vertical Test Rig

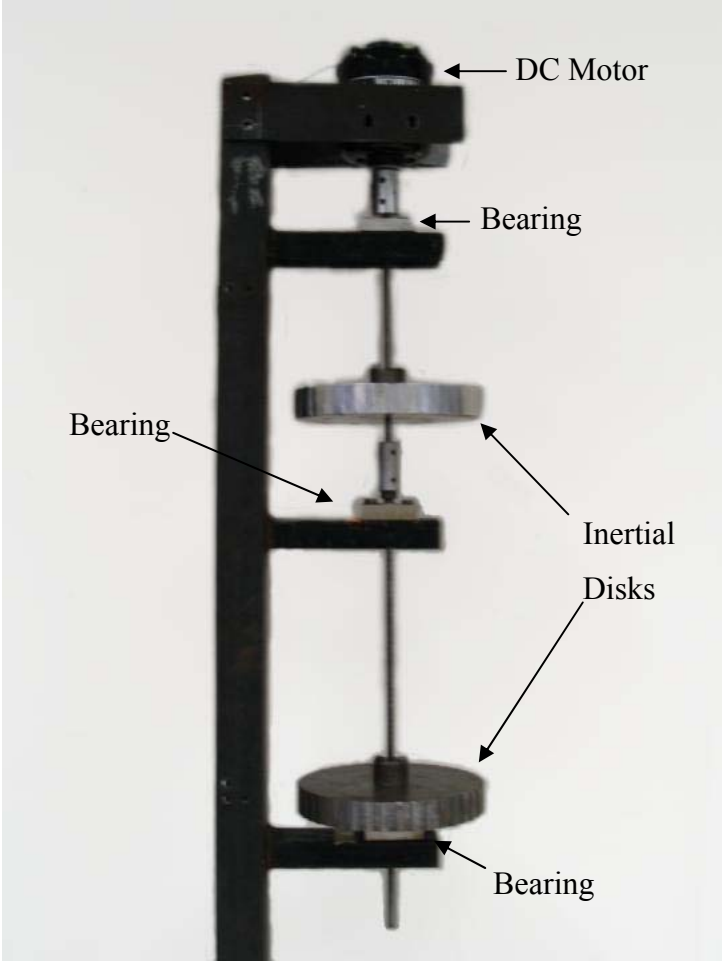

Figure 23: Vertical torsional test rig

The vertical test rig is comprised of a long slender shaft with two massive disks shown in Figure 23. The system is driven by a universal motor that can be powered

from either an AC or DC signal; for this application, a DC power supply was used. The electric motor is attached to the shaft via a rigid coupling. The shaft going from the coupling to each of the two disks is a rod of cold rolled steel. The steel circular disks can be positioned at different points along the shaft and held in place by a set screw. Three bearings are placed along the shaft to hold the system in place. The bearings are rolling element bearings and have negligible inertial mass compared to the disks. A table describing the properties of each element of the test rig is displayed in Table 1.

Table 1: Properties of the Vertical Test Rig.

Element	Weight (lb)	Length (in)	Diameter (in)	Inertia (lb*in^2)
Motor/Coupling	1.10	5.75	2.125	0.8553
Shaft	0.333	24	0.25	0.00261
Top Disk	9.35	1	6.5	49.38
Bottom Disk	9.26	1	6.5	47.58

The inertia of the disk was experimentally determined. Conkey in [13] attached a series of metal strips using aluminum tape to the top disk; twenty eight strips are spaced as close to equally apart as possible. These strips act as an encoder in order to pick up the instantaneous speed of the rotating system. A carrier pulse signal was generated using a BK MM0002 magnetic probe as seen in Figure 24.

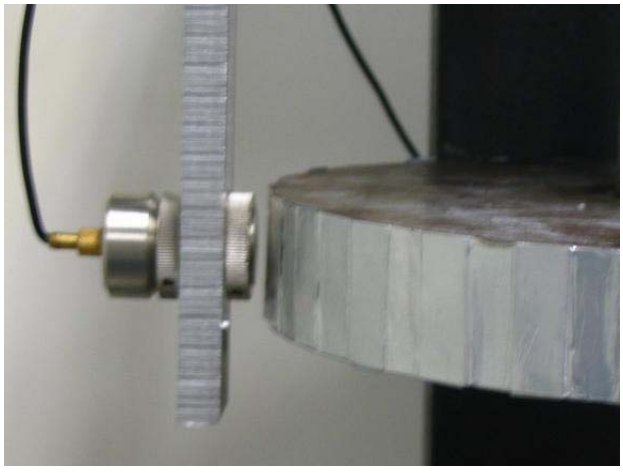

Figure 24: Magnetic transducer with metal strip encoder.

Forty, quarter-inch segments were machined from the bottom disk creating an encoder. This encoder is more accurate than the one created for the top disk due to the high precision procedure used in machining the segments. A carrier signal was created using an eddy-current proximity probe as shown in Figure 25.

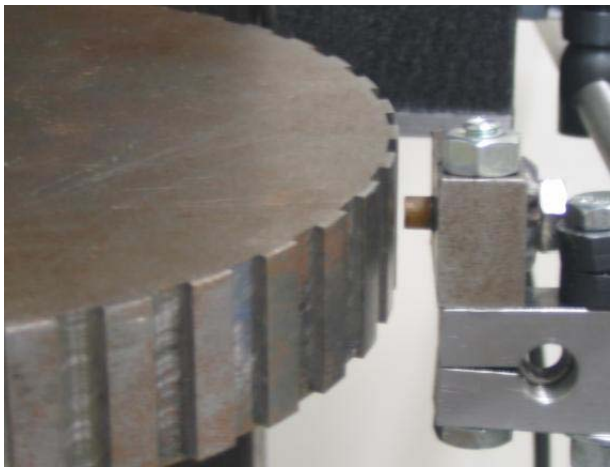

Figure 25: Proximity probe with machined slotted encoder.

Modeling of the Vertical Test Rig

The Vertical Test Rig system was modeled in order to determine the torsional natural frequency. A model of the Vertical Test Rig is displayed in Figure 26.

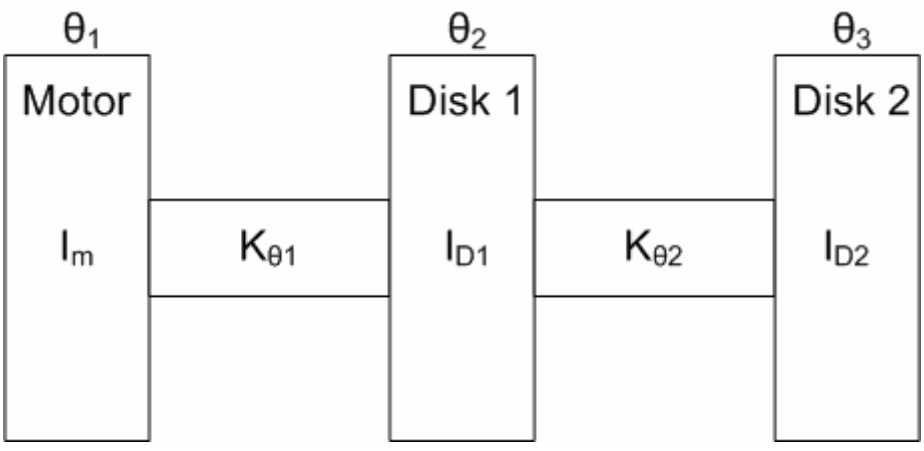

Figure 26: Model of Vertical Test rig.

The model consists of the inertia from the two disks and the motor/coupling along with the torsional stiffness of each shaft section. There is little damping in the system,

therefore it is neglected in the model. The equations of motion for the model of the Vertical test rig are the following:

$$\begin{aligned} I_m\ddot{\theta}_1 + K_{S_1}\left(\theta_1 - \theta_2\right) &= 0 \\ I_{D_1}\ddot{\theta}_2 + K_{S_1}\left(\theta_2 - \theta_1\right) + K_{S_2}\left(\theta_2 - \theta_3\right) &= 0 \\ I_{D_2}\ddot{\theta}_1 + K_{S_2}\left(\theta_3 - \theta_2\right) &= 0 \end{aligned} \tag{23}$$

The torsional shaft stiffness of each section is given by [1]:

$$K_{S_n} = \frac{J_n G}{l_n} \tag{24}$$

where J_n is the polar moment of the shaft, G is the shear modulus, and l_n is the shaft section length. The solutions to the equations of motion in Equation 23 are:

$$\begin{aligned} \theta_1 &= A_1 e^{st} \\ \theta_2 &= A_2 e^{st} \\ \theta_3 &= A_3 e^{st} \end{aligned} \tag{25}$$

where A_n are constants and the values for s are the complex conjugate eigenvalues. Plugging the solutions into the equations of motions yields the following:

$$\begin{pmatrix} I_m s^2 + K_{S_1} & -K_{S_2} & 0 \\ -K_{S_1} & I_{D_1} s^2 + K_{S_1} + K_{S_2} & -K_{S_2} \\ 0 & -K_{S_2} & I_{D_2} s^2 + K_{S_2} \end{pmatrix} \bullet \begin{pmatrix} A_1 \\ A_2 \\ A_3 \end{pmatrix} = \begin{pmatrix} 0 \\ 0 \\ 0 \end{pmatrix} \tag{26}$$

The eigenvalues of the system, s, are solved by taking the determinant of the matrix in Equation 26 and setting it equal to zero. Since damping is neglected in the system, there will only be imaginary numbers for the value of the eigenvalues. The imaginary part of the eigenvalues is the natural frequency of the system. Using the properties of the Vertical Test rig found in Table 1, the natural frequencies of the system were calculated to be the following:

$$\begin{aligned} \omega_{\theta_n} &= 0 \\ &= 11.379 \quad (Hz) \\ &= 412.429 \end{aligned} \tag{27}$$

Description of the T-L Test Rig

The torsional-lateral (T-L) Rig, developed by Rajagopalan in [14], consists of two parallel shafts mounted on ball bearings without any support flexibility option; the test rig is displayed Figure 27.

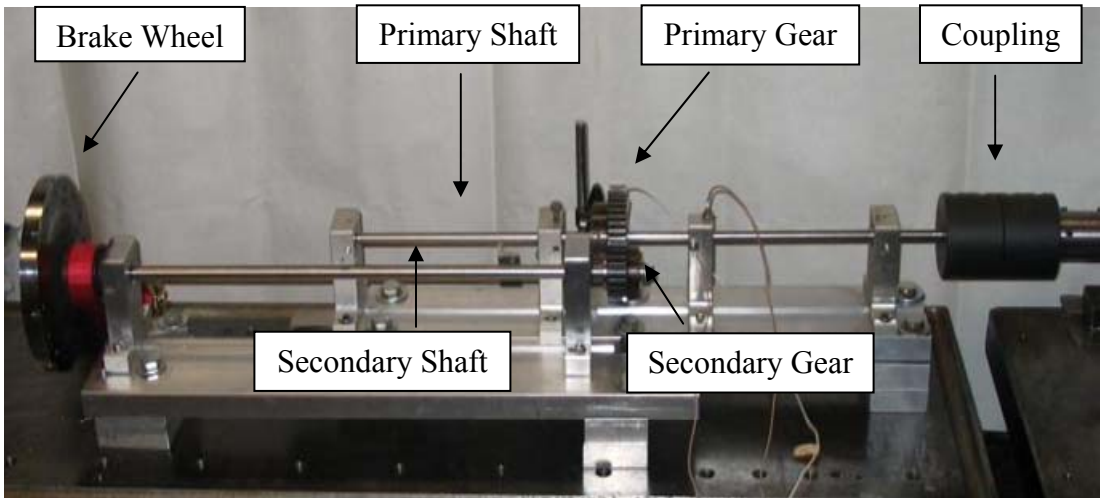

Figure 27: The T-L test rig.

The primary gear is mounted on the primary shaft and held in position with two diametrically opposite set screws. The primary shaft is supported on three ball bearings and is driven by a DC motor through a torsionally rigid coupling. The secondary shaft is supported on two ball bearings and has overhung masses at both ends. At one end of the shaft, the secondary gear transmits power from the primary shaft. The gear ratio between the primary and secondary gears is 1.75 [14]. At the other end, a band is wrapped around a brake wheel to provide the necessary load to keep the gears in contact. The brake wheel acts as a large inertia to keep the first torsional natural frequency low while serving as a surface for the band to apply a load [14]. Both the primary and secondary rotors are mounted on flat aluminum bases. Alignment between the bearing housings and the shaft separation distance is ensured through machined keyways [14]. Figure 28 displays the two gears meshed together along with the brake wheel.

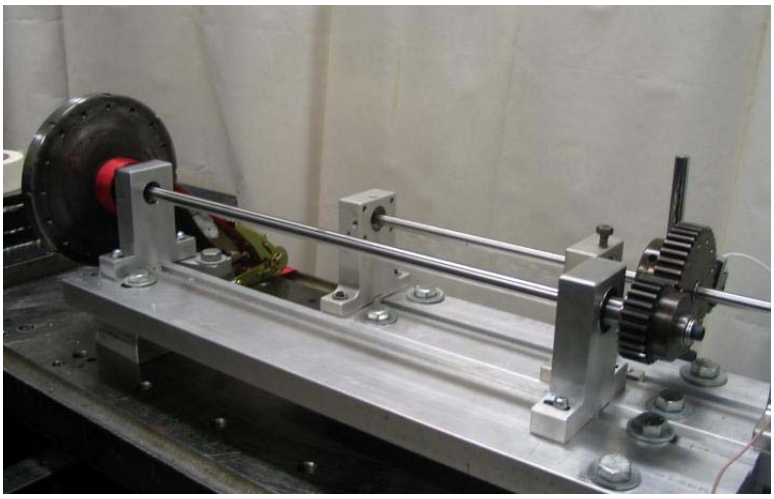

Figure 28: Meshed gears and brake wheel of the T-L test rig.

Forty-two slots were machined from the brake wheel producing an encoder with minimal error in segment spacing. The two gears and the brake wheel are used as encoders and an eddy-current proximity probe is used for generating the carrier signal. Figure 29 displays a proximity probe mounted near the primary gear for speed pickup.

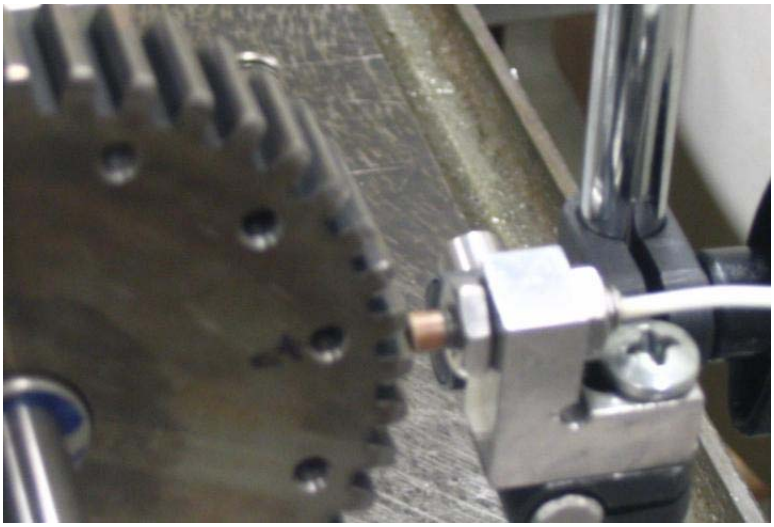

Figure 29: Proximity probe mounted near primary gear.

The properties for each element of the T-L test rig are given in Table 2.

Table 2: Properties of element of the T-L test rig [14].

Element	Length (in)	Diameter (in)	Inertia (lb*in^2)
Motor (rotor)	23	1.25	272.178
Coupling	4	3	
Primary Shaft	11	0.375	___
Secondary Shaft	22	0.5	___
Primary Gear	1.375	3.5	5.338
Secondary Gear	1.25	2	
Brake Wheel	2.2	7	148.134

Modeling of the T-L Test Rig

Rajagopalan in [14] modeled the T-L test rig to determine torsional natural frequencies of the system. A schematic of the model is displayed in Figure 30.

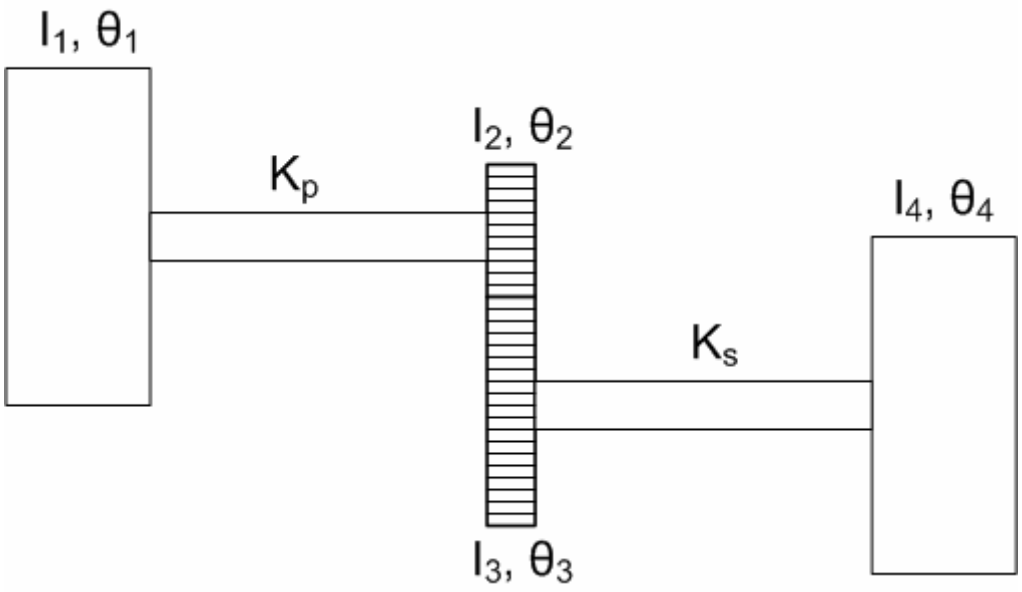

Figure 30: Model of the T-L test rig.

The model consists of the inertia of the motor (I_1), the primary gear (I_2), the secondary gear (I_3), and the brake wheel (I_4). The inertia of the primary and secondary shaft is

neglected; their torsional stiffness is represented as K_p and K_s respectively. The equations of motion for the T-L test rig are given as the following [14]:

$$\begin{aligned} I_1\ddot{\theta}_1 + K_p\left(\theta_1 - \theta_2\right) &= 0 \\ \left(I_2 + N^2 I_3\right)\ddot{\theta}_2 + K_p\left(\theta_2 - \theta_1\right) + N^2 K_s\left(\theta_2 - \frac{\theta_4}{N}\right) &= 0 \\ N^2 I_4 \frac{\ddot{\theta}_4}{N} + N^2 K_s\left(\frac{\theta_4}{N} - \theta_2\right) &= 0 \end{aligned} \tag{28}$$

where N is the gear ratio. Substituting θ_4' for $\frac{\theta_4}{N}$ yielded the following [14]:

$$\begin{pmatrix} I_1 & 0 & 0 \\ 0 & I_2 + NI_3 & 0 \\ 0 & 0 & N^2 I_4 \end{pmatrix} \bullet \begin{pmatrix} \ddot{\theta}_1 \\ \ddot{\theta}_2 \\ \ddot{\theta}_4' \end{pmatrix} + \begin{pmatrix} K_p & -K_p & 0 \\ -K_p & K_p + N^2 K_s & -NK_s \\ 0 & -NK_s & N^2 K_s \end{pmatrix} \bullet \begin{pmatrix} \theta_1 \\ \theta_2 \\ \theta_4' \end{pmatrix} = \begin{pmatrix} 0 \\ 0 \\ 0 \end{pmatrix} \tag{29}$$

Using the process for solving for the eigenvalues described for the Vertical test rig, the torsional natural frequencies for the T-L test rig were calculated to be the following [14]:

$$\begin{aligned} \omega_{\theta_n} &= 0 \\ &= 12.014 \quad (Hz) \\ &= 140.56 \end{aligned} \tag{30}$$

CHAPTER IV
THE MEASUREMENT TEST STAND AND PROCEDURES

All the data acquisition was carried out on an Intel Pentium 4, 1.7 GHz personal computer with Windows®NT operating system, 1.5 GB RAM and 40 GB of hard drive space. The computer is equipped with LabVIEW 8.2 Development System along with two National Instruments PCI 4472 DAQ boards. The National Instruments PCI-4472 is an eight-channel dynamic signal acquisition board for making high-accuracy frequency-domain measurements [15]. It has a 24-bit resolution with a 110 db dynamic range. It has the capability of sampling 8 analog inputs at up to 102.4 kS/s. The 4472 board is displayed in Figure 31 [15].

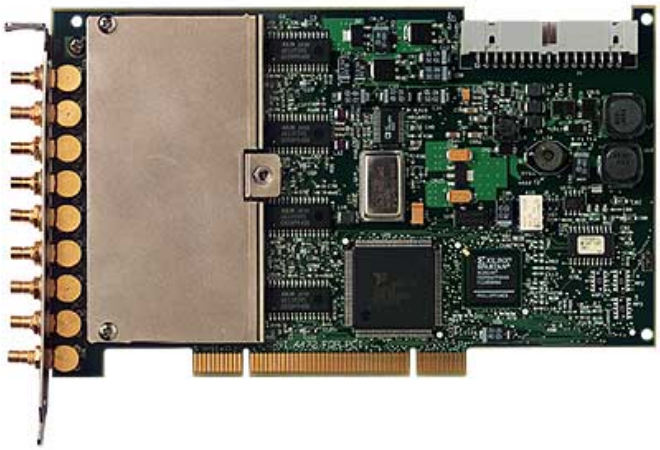

Figure 31: PCI 4472 DAQ board.

As stated previously, eddy-current proximity probes and a BK MM0002 magnetic probe were used to generate pulses from encoders. The proximity probe signal, powered by an 18V power supply, was fed into the DAQ board via a SMB to BNC connector, which AC coupled the signal. The magnetic probe requires no power source and was fed directly into the DAQ board via the SMB to BNC connector.

LVTorsion – The Measurement System

Using the theory explained in the METHODOLOGY, a LabVIEW™ Virtual Instrument (VI) was developed to test the effectiveness of each method in reducing the noise generated in the shaft speed signal. Once the external hardware has been set-up properly, the virtual channels of the program must be configured. The channel configuration page is displayed in Figure 32.

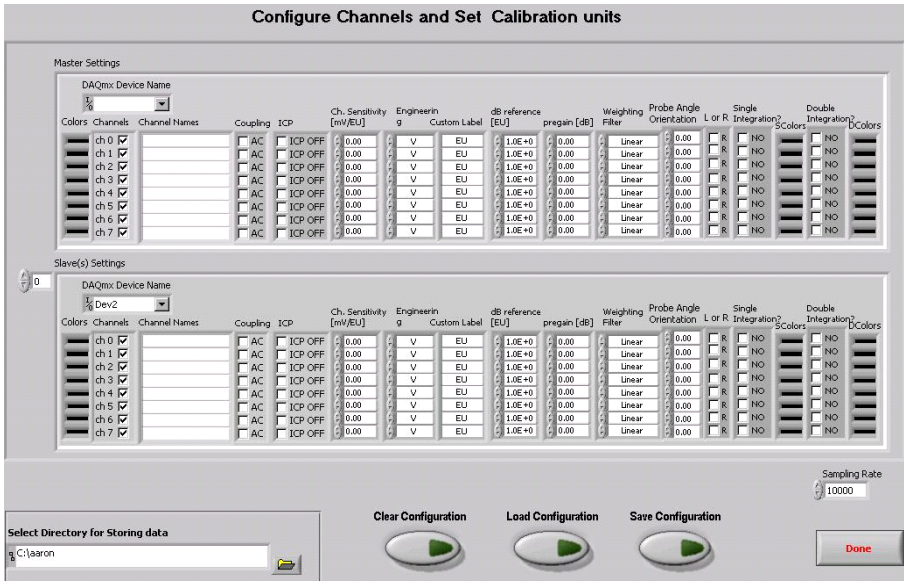

Figure 32: Virtual channel configuration.

The channel configuration page allows the user to set the attributes of the measurement probes, the sampling rate of the DAQ devices, and the location to save the data being acquired. After the virtual channels have been configured, the VI begins acquiring data coming from the measurement probe. The front panel of the VI is displayed in Figure 33.

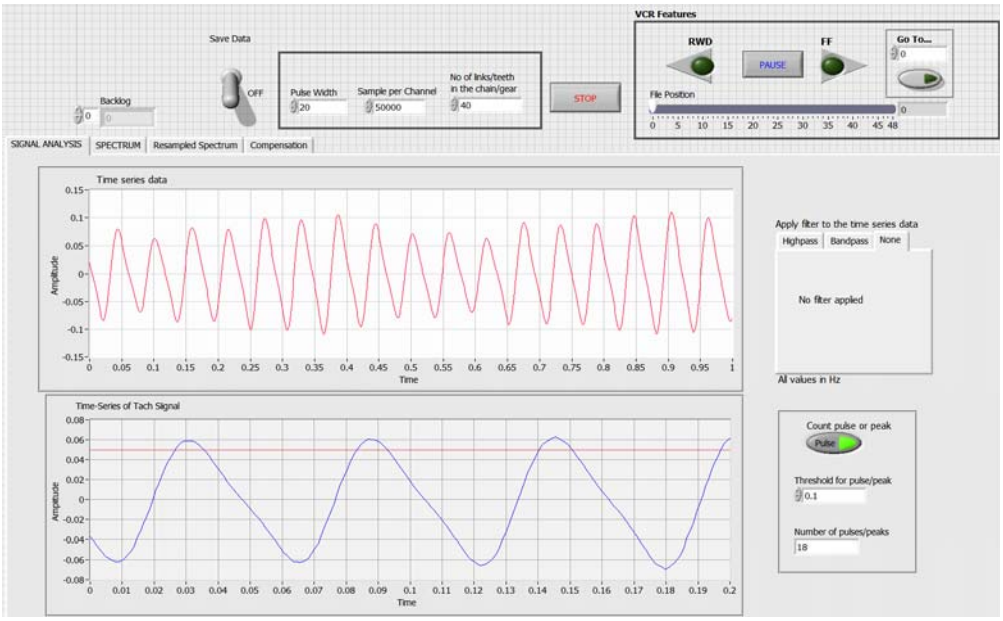

Figure 33: Front panel of the torsional measurement system.

The front panel consists of functions that allow the user to set the number of pulses per revolution of the carrier signal, the number of samples to acquire in a given time block, and the minimum number of data points that must be in a given pulse. The main portion of the front panel is a tabular page that contains the results of the various measurement techniques. The various tabs include: Signal Analysis, Spectrum, Resampled Spectrum, and Compensation.

The 'Signal Analysis' page displays the graph of the carrier signal. On this page the user sets the threshold level that each pulse must meet in order for it to be used in the speed calculation process. The user also has the option to filter the signal via a high-pass filter or a band-pass filter. For the work done in this thesis, a filter was not used. The 'Signal Analysis' page is displayed in Figure 34.

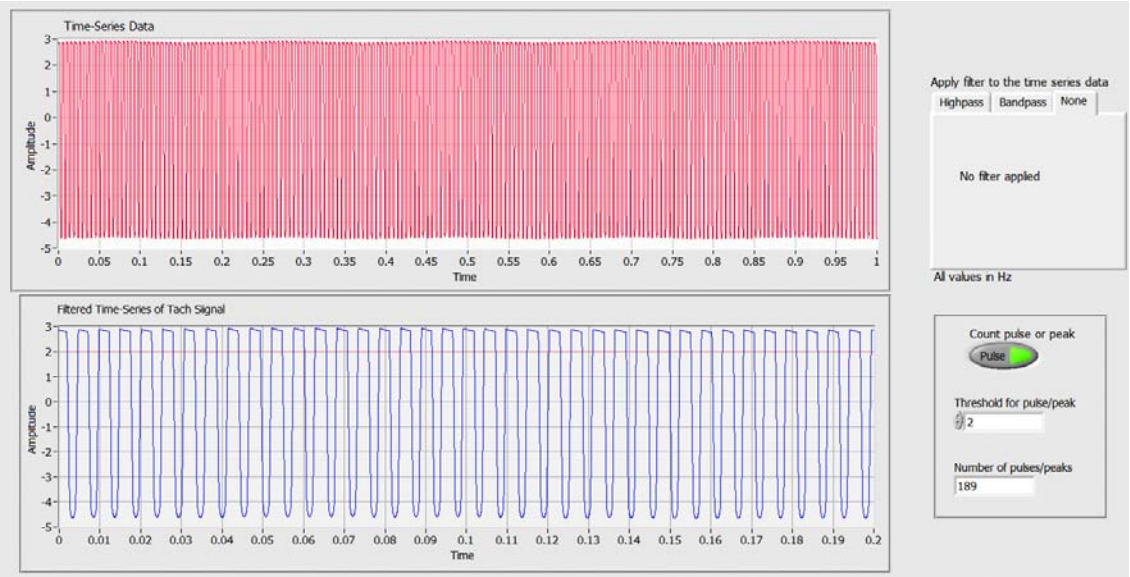

Figure 34: 'Signal Analysis' tab.

The ‘Spectrum’ page contains signal of the computed speed of the shaft. Frequency spectrums of of the shaft speed and of the carrier signal are also displayed on this tab. A set of averaging parameters and a windowing function allows the user to clean up the spectrums as much as possible. The ‘Spectrum’ page is displayed in Figure 35.

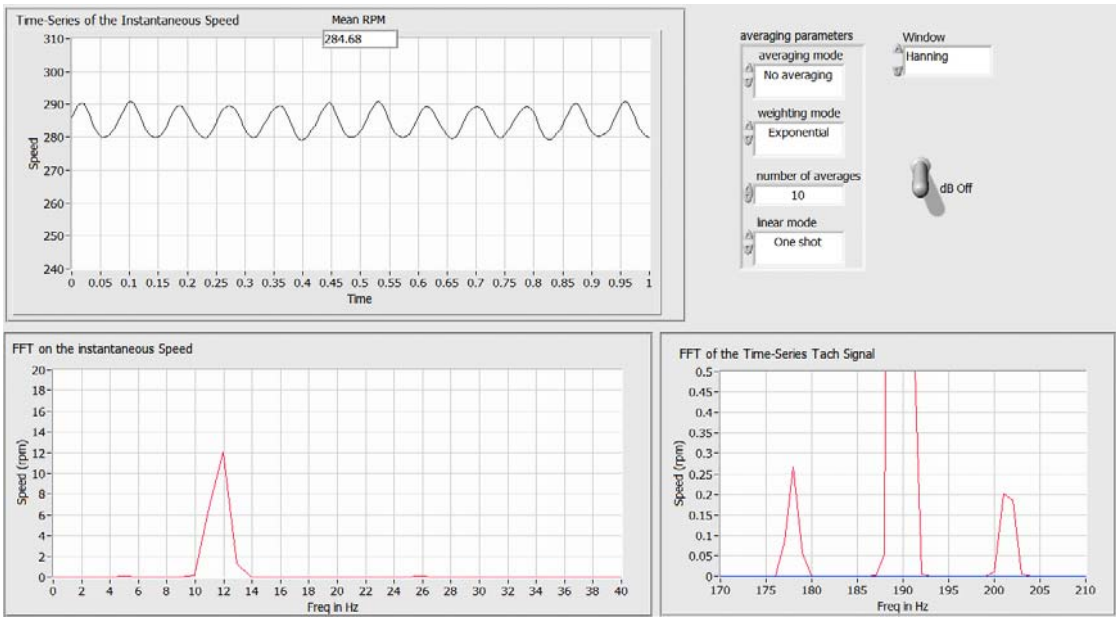

Figure 35: 'Spectrum' tab.

The ‘Resampled Spectrum’ page contains the graph of the instantaneous speed resampled into the order domain along with its order spectrum. Accompanying these two graphs is a graph of the order spectrum with the order components of the running speed removed from the signal. The ‘Resampled Spectrum’ page is displayed in Figure 36.

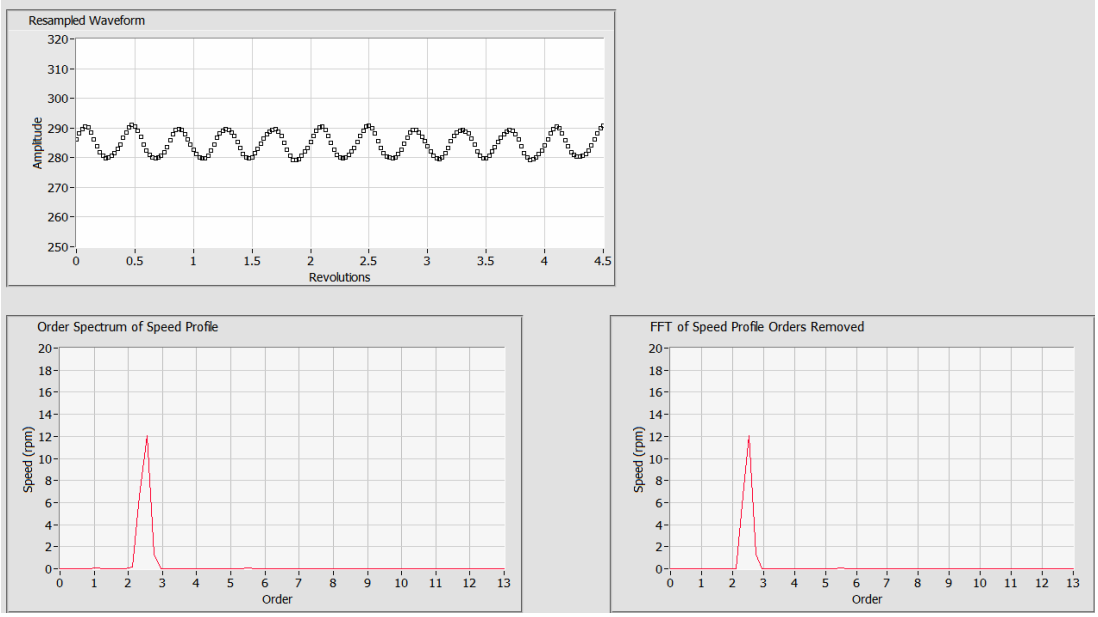

Figure 36: 'Resampled Spectrum' tab.

The ‘Compensation’ tab is the last page of the tabular list and consists of the graph of the shaft speed after it has been geometrically compensated. A frequency spectrum of the compensated speed is also displayed. A numeric control of the speed upper bound allows the user to determine the maximum frequency of interest to view on the spectrum. The ‘Compensation’ tab is displayed in Figure 37.

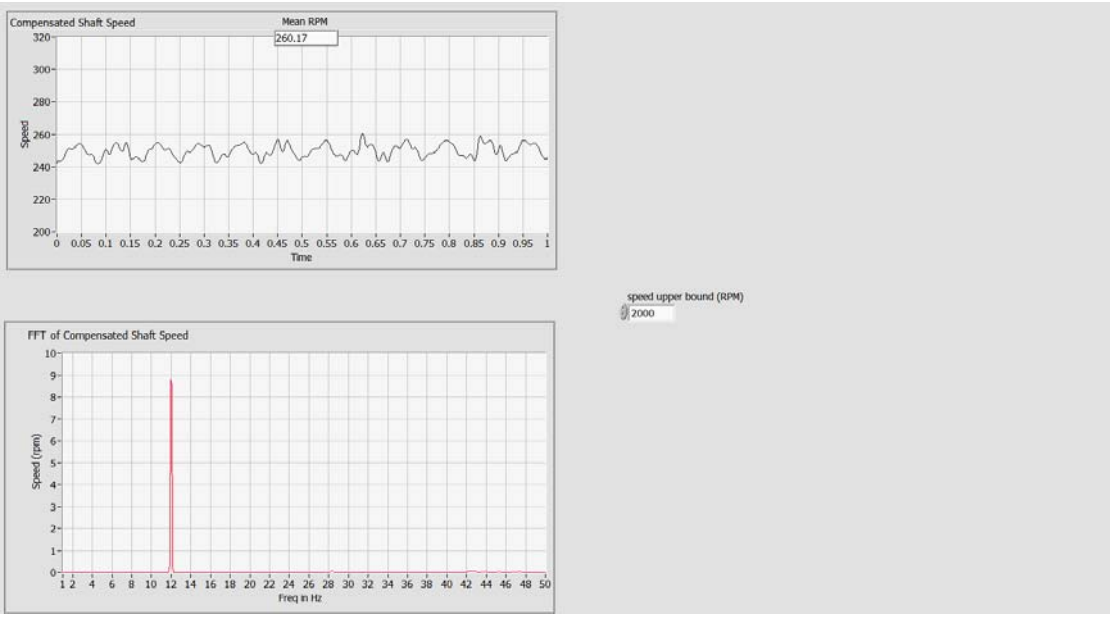

Figure 37: 'Compensation' tab.

Measurement Procedure

Steady-state and transient tests were conducted in order to determine the effectiveness of the measurement techniques, discussed in the METHODOLOGY, in measuring torsional vibration. The majority of the tests were conducted on the Vertical test rig, while tests performed on the T-L test rig were used to further validate the results found from the Vertical test rig. On the Vertical test rig, torsional vibration was measured on both disks. The encoders of the two disks vary in number of segments along with their accuracy. The encoder on the bottom disk was purposely manufactured at a higher tolerance in order to compare the noise generated from encoder inaccuracies. On the T-L test rig, torsional vibration was measured at the two gears along with the brake wheel. All measurements were taken using either the LabVIEW program developed for this thesis or the program developed by Kar discussed in the Background Research section. As stated previously, Kar's torsional vibration measurement program was used as a baseline measurement for which all other measurement techniques were compared to.

Torsional Excitation

Torsional vibration was excited in the Vertical test rig by superimposing an AC signal on the DC signal supplied to the motor. The result is the variation in the voltage supplied to the motor thus causing a speed fluctuation in the system. The superimposing of the AC signal was accomplished by connecting the DC power supply and the motor in series with a function generator. In order to achieve appreciable amplitudes for the AC signal, the signal from the function generator was sent into a power amplifier before connecting to the circuit.

Torsional vibration was excited in the T-L test rig by supplying an AC signal to the field windings of the DC motor used. The speed of the motor was controlled through the armature current. The AC signal was generated via a function generator and a power amplifier was used to amplify the signal.

Steady-State Testing

The Vertical test rig was limited to test runs at speeds lower than the calculated torsional natural frequency of around 12 Hz due high shaft misalignment and imbalance in the system. It was found that running the rotor passed 720 rpm resulted in an unacceptable level of vibrations in the system. Therefore, steady-state testing was limited to speeds at 300 and 360 rpm. While running at these selected speeds, a constant 12 Hz excitation was applied to the system. The sampling frequency of the data acquisition board was varied while running at a speed around 300 rpm. The range of sampling frequencies used includes the following (in kHz): 1, 1.5, 2, 3, 5, 10, 20, 50 and 100. By varying the sampling frequency, the affect it has on the accuracy in calculating the shaft speed was determined.

A typical steady-steady test measurement was performed by first taking the shaft speed to the selected running speed while running the LabVIEW program at the selected sampling frequency. Once the selected speed was reached, data was saved in the LabVIEW program. The program continued saving for some time without exciting any torsional vibration in order to observe the noise generated in the system. After a few moments, a 12 Hz torsional excitation was introduced in the system and its affects were

observed in the LabVIEW program. Once an adequate amount of data was taken, the LabVIEW program was stopped and the Vertical test rig was shut down. The LabVIEW program has the ability to playback the data files in order to closely observe the effectiveness of each torsional vibration measurement technique.

Transient Testing

Due to the limitations of the Vertical test rig stated in the Steady-State Testing section, transient testing was limited to a speed range from 200 to 500 rpm. During a transient test, a constant 12 Hz torsional excitation was applied to the system. The sampling frequency of the data acquisition board held constant during transient testing. The effect of varying speeds on the different measurement techniques was observed.

A typical transient test began with running the rotor up to 200 rpm while starting the LabVIEW program. Once the desired speed was reached, the LabVIEW Program began saving data. The rotor speed was then increased rapidly without any external torsional excitation; the transient behavior was observed.

Experimental Verification

As stated previously, the T-L test rig was used to verify the capability of the measurement techniques in reducing the noise in the torsional vibration measurement. Testing of the T-L test rig began with a transient start-up test where the secondary shaft speed was rapidly increased from zero to a selected speed of 2300 rpm (1314 rpm for primary shaft). A start-up test was performed with a constant 11 Hz torsional excitation. Once the selected speed of 2300 rpm was reached, steady-state testing at an 11 Hz excitation frequencies ensued. The selected speed of 2300 rpm was used because it was well beyond the torsional natural frequency of the system. All of the testing for the Vertical test rig was performed at speeds lower than the torsional natural frequencies. It was desired to observe the affect of running at speeds higher than the torsional natural frequency on the measurement system.

CHAPTER V
RESULTS AND DISCUSSION

Before testing the effectiveness of the measurement techniques in reducing the noise, a few things needed to be confirmed: (1) the assumption that encoder spacing errors are a source of noise, (2) these spacing errors are present in one of the encoders used in the testing, (3) the torsional excitation signal from the signal generator excites torsional oscillations in the system at that same frequency.

Spacing Error Confirmation

As stated previously, a major source of error in measuring shaft speed is the variation in the lengths of encoder segments. Varying encoder lengths will appear as speed fluctuations. When using the TIMS method for calculating torsional vibration, any speed fluctuation will appear in the frequency spectrum of the shaft speed. These artificial fluctuations in the shaft speed mask important frequencies, such as torsional vibration. It was assumed that the encoder machined into the bottom disk of the Vertical test rig was more accurate than the taped metal strips attached to the top disk. In order verify this assumption, the angle-interval of each encoder segment was calculated for both encoders. This method was performed by running the test rig at a constant speed (between 150 and 250 rpm) with no external torsional excitation. Once the shaft speed was constant, the time-interval for each encoder segment was averaged over 30 revolutions. Using a once per revolution tachometer signal as a reference, each encoder segment was identified. Taking the average shaft speed over the 30 revolution time period, the angle-interval was calculated using the following:

$$\theta_i = \omega_{avg} \cdot \Delta t_{i,avg} \left(\frac{180}{\pi} \right) \text{ (deg)} \tag{31}$$

where ω_{avg} is the average shaft speed in rad/sec and $\Delta t_{i,avg}$ is the average time-interval of each encoder segment.

The angle-interval for each segment of the top disk encoder (metal strips) is displayed in Figure 38.

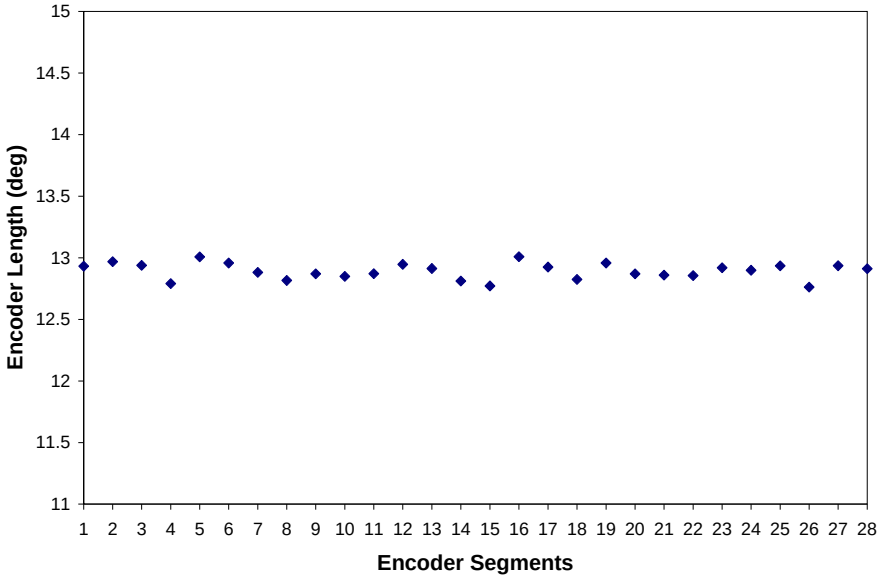

Figure 38: Length of encoder segments for the top disk encoder.

This encoder has 28 segments; if the spacing of encoder segments were equal, then the length of each segment would be 360/28 or 12.857°. The highest percent deviation from the average angle-interval for each encoder segment was less than 3%.

The angle-interval for each segment of the bottom disk encoder (machined segments) is displayed in Figure 39.

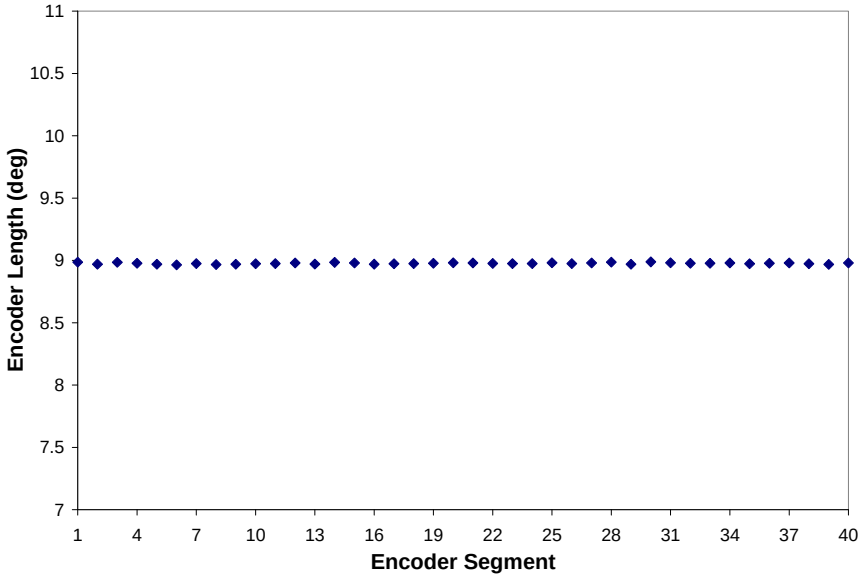

Figure 39: Length of encoder segments for the bottom disk encoder.

This encoder has 40 segments; if the spacing of encoder segments were equal, then the length of each segment would be 360/40 or 9°. The highest percent deviation from the average angle-interval for each encoder segment was less than 0.3%. The results shown in Figure 38 and Figure 39 confirm the assumption made about the accuracy of each encoder. The variation in encoder length for the bottom disk encoder is minimal while the variation in encoder length for the top disk encoder is extremely noticeable.

Because variations in encoder length occurs every revolution, these length variations manifest themselves as speed fluctuations at frequencies equal to the harmonics of the shaft speed. To demonstrate this affect, the Vertical test rig was held at a constant speed of around 250 rpm with no external torsional excitation. A carrier signal was generated using the top disk encoder. From the LVTorsion measurement system, the frequency spectrum of the instantaneous shaft speed is displayed in Figure 40.

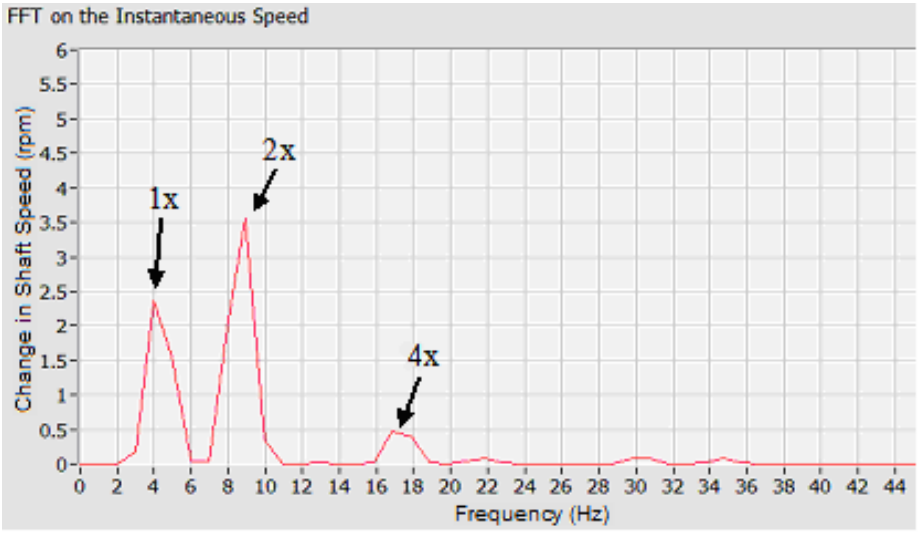

Figure 40: FFT of shaft speed no torsional excitation (top disk encoder).

The average running speed of the shaft was around 260 rpm. In comparison, the frequency spectrum for the bottom encoder at a constant running with speed no torsional excitation is displayed in Figure 41.

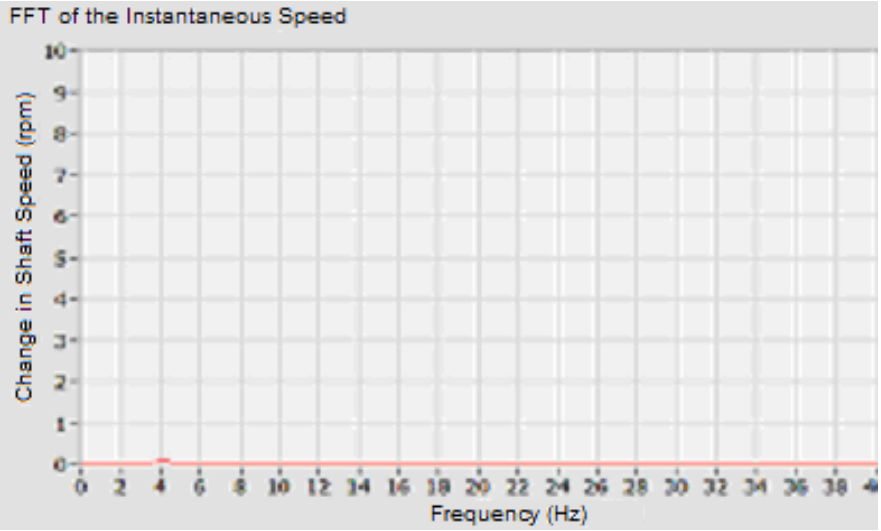

Figure 41: FFT of shaft speed no torsional excitation (bottom encoder).

The average running speed of the shaft was around 260 rpm. The harmonics of the shaft speed practically disappear when measuring shaft speed with an accurately spaced encoder.

Torsional Excitation Confirmation

Torsional oscillations were excited in the Vertical test rig by connecting a signal generator via a power amplifier in series with the DC power supply and the motor. The frequency of the oscillating signal was chosen to be around 12 Hz, the calculated torsional natural frequency, because less power was required for torsional excitation. To confirm that the 12 Hz signal from the signal generator was exciting the system at 12 Hz, the TIMS method and side-band method were used in tandem. The machined encoder on the bottom disk was used to generate the carrier signal in order to minimize the noise from encoder spacing errors. The shaft speed was held at a constant running speed of around 280 rpm and the sampling frequency of the DAQ board was set to 50 kHz. With no external torsional excitation, the frequency spectrum of the shaft speed showed no dominant peaks at any frequency. These results were confirmed from frequency spectrum of the carrier signal. There were no apparent side-bands around the tooth passing frequency. Once no torsional oscillations were confirmed, the power from the amplifier was increased. The plot of the shaft speed is displayed in Figure 42.

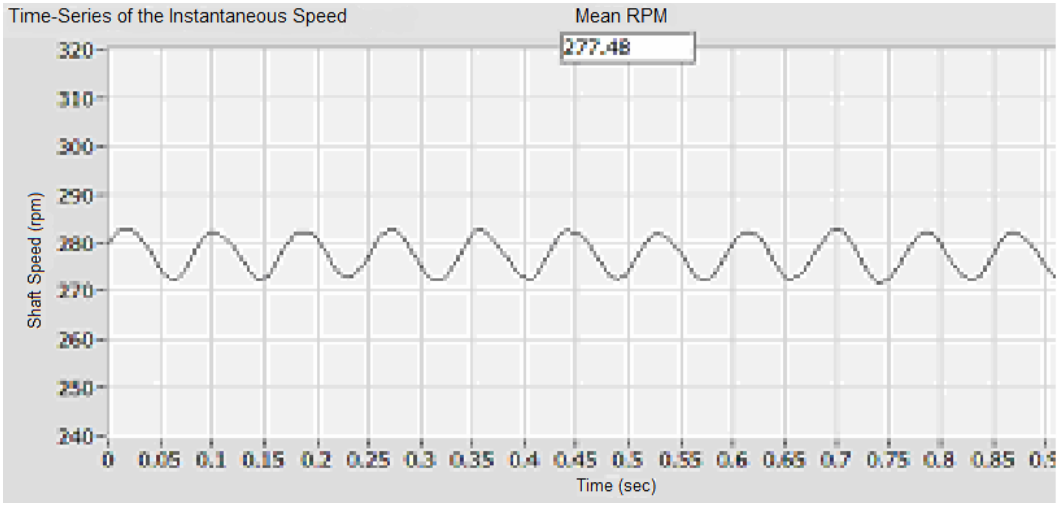

Figure 42: Plot of shaft speed with a 12 Hz excitation using machined encoder.

A speed fluctuation at a certain frequency is evident in this graph. The frequency spectrum of this signal is displayed in Figure 43.

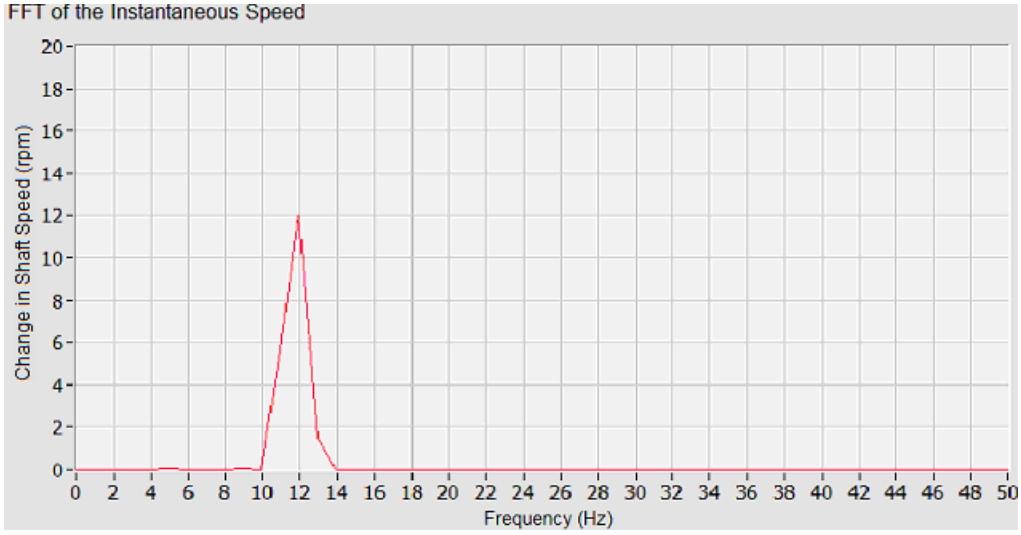

Figure 43: Frequency spectrum of shaft speed with a 12 Hz excitation.

The frequency of the speed fluctuation was 12 Hz, the same as the frequency from the signal generator. The torsional oscillating frequency was verified on the frequency spectrum of the carrier signal shown in Figure 44.

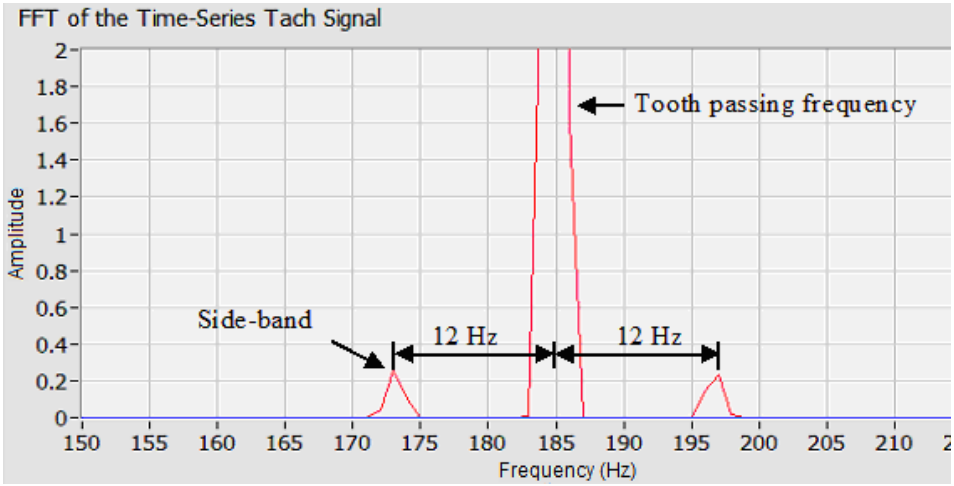

Figure 44: Frequency spectrum of carrier signal with 12 Hz side-bands.

Speed Calculation

Steady-state and transient testing were performed on the vertical test rig in order to determine the effectiveness of the shaft speed algorithm, discussed in the METHODOLOGY, in reducing the noise generated in the signal of the shaft speed. Kar's measurement system was used a baseline for which the results of using new shaft speed algorithm was compared to. In order to make a proper comparison between the two methods, the same data file in LabVIEW was played back on both programs.

Steady-State Testing

Steady-state testing was performed on the Vertical test rig at a speed between 250 and 300 rpm with a constant 12 Hz torsional excitation. The carrier signal was generated using the magnetic probe and the taped, metal strip encoder on the top disk of the test rig. The carrier signal was sampled at a 50 kHz sampling frequency with 50000 samples in a time block.

Kar's measurement system yielded the signal of the shaft speed displayed in Figure 45.

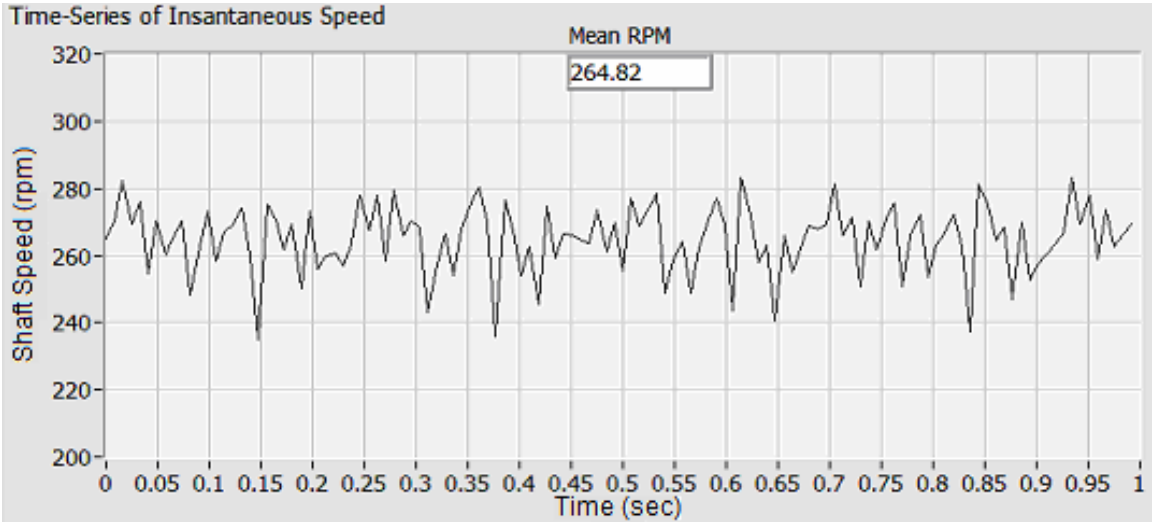

Figure 45: Signal of shaft speed using Kar's measurement system at steady-state speed.

The signal generated showed speed fluctuations at multiple frequencies; this is evident in the frequency spectrum displayed in Figure 46. The only fluctuating frequency should have been the 12 Hz frequency from the signal generator.

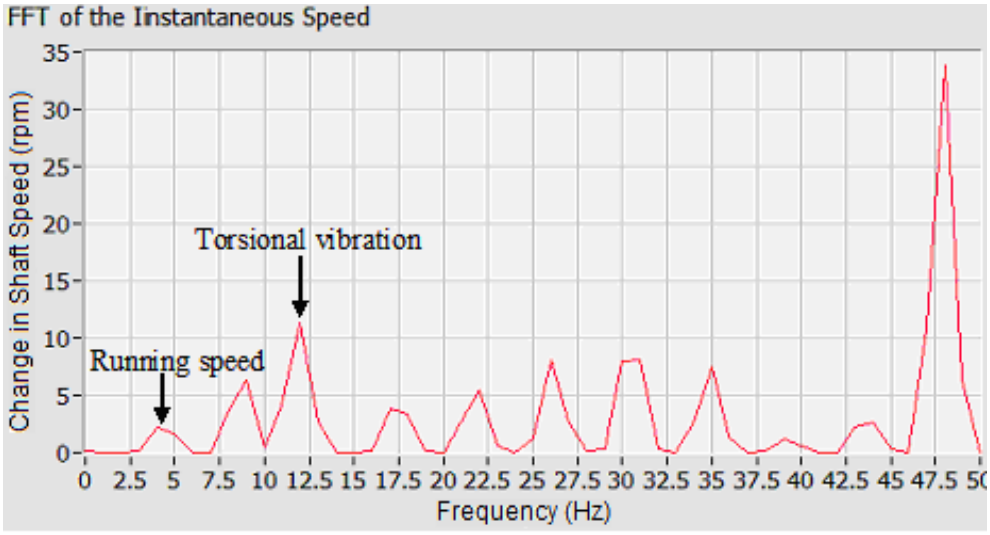

Figure 46: FFT of shaft speed using Kar's system at steady-state speed.

Many of these frequencies occurred at harmonics of the shaft speed of 4.4 Hz. As demonstrated earlier, the source of some of these harmonic frequencies comes from inaccuracies in encoder spacing. Some of the extreme changes in speed could have

come from missing pulses in the calculation algorithm. This algorithm counted the number of pulses that occur in a specified time period, which runs the risk of being between pulses at the end of the time period. Missing pulses appear as abrupt changes in speed.

In order to confirm this hypothesis, the same data file was used with the new speed calculation algorithm. The results yielded the signal of the shaft speed displayed in Figure 47.

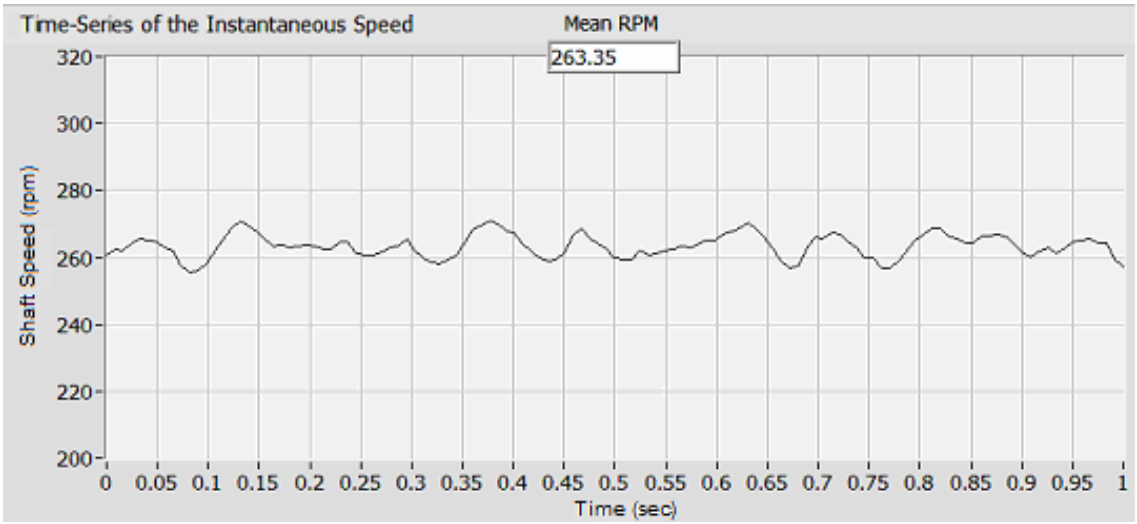

Figure 47: Signal of shaft speed using LVTorsion at steady-state speed.

This graph showed fewer speed fluctuating frequencies than the one shown in Figure 45. The result was a cleaner frequency spectrum shown in Figure 48.

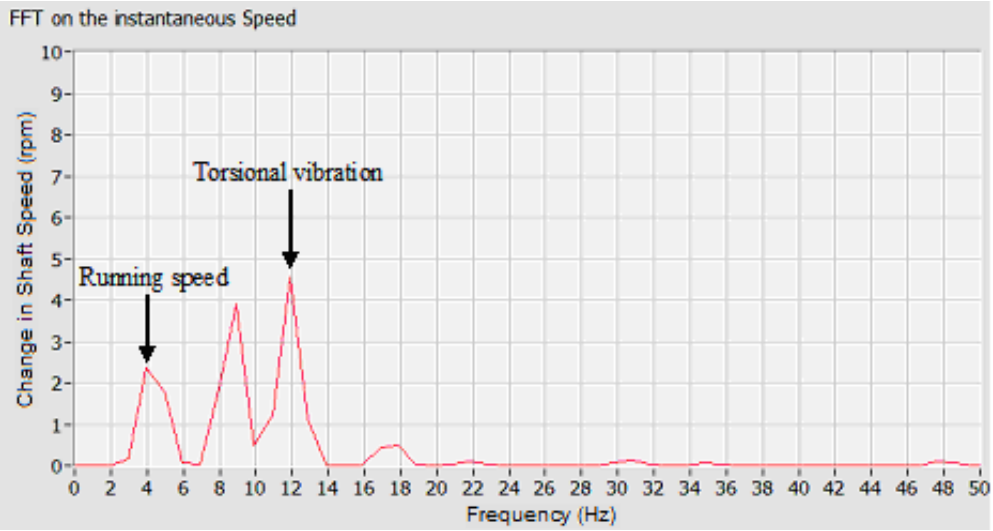

Figure 48: FFT of shaft speed using new LVTorsion at steady-state speed.

A few harmonics of the shaft speed still appear in the spectrum but most of the high order components were eliminated. Because this calculation method used the pulse width of each encoder segment to calculate shaft speed, the chance of missing pulses is dramatically reduced. As a result, the noise generated in the signal of the shaft speed was reduced.

Transient Testing

Transient testing was performed on the Vertical test rig starting at a speed of 200 rpm and going up to 500 rpm with a constant 12 Hz excitation. The speed was not taken any higher than 500 rpm because of the high lateral vibrations due to imbalance and shaft misalignment. High lateral vibrations could affect the measurement of pulse positions from the encoder. As with steady-state testing, the carrier signal was generated using the magnetic probe and the taped, metal strip encoder on the top disk of the test rig. The signal was sampled at a 50 kHz sampling frequency with 50k samples in a given time block.

Figure 49 displays the graph of the shaft speed from Kar's measurement system with the shaft speed ramping up to 500 rpm.

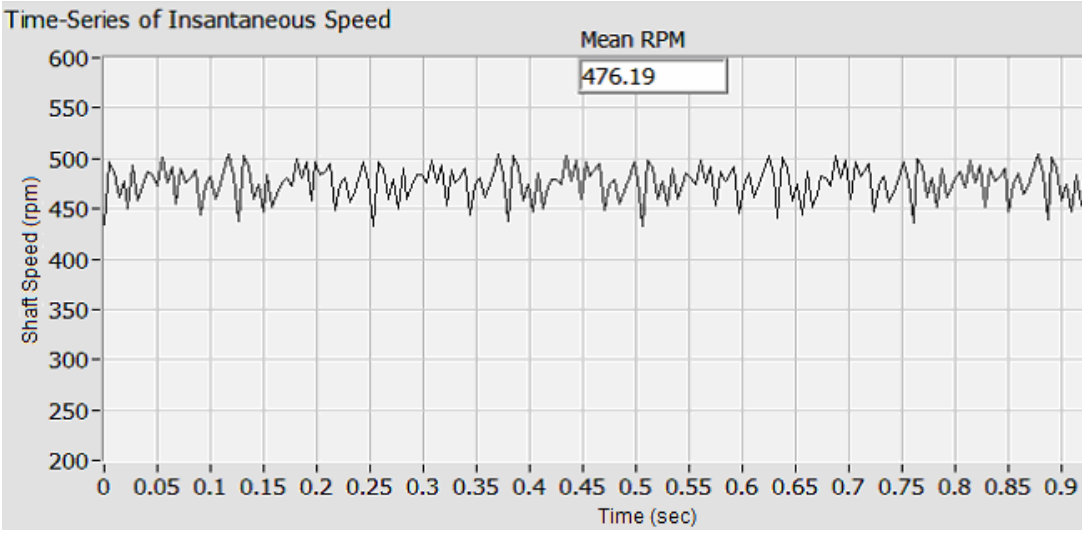

Figure 49: Signal of shaft speed using Kar's method at transient speeds.

As in Figure 45, the signal displayed speed fluctuations at multiple frequencies. The only frequency that should have been seen was the 12 Hz frequency coming from the function generator. The multiple frequency components of the signal manifested themselves in the frequency spectrum displayed in Figure 50.

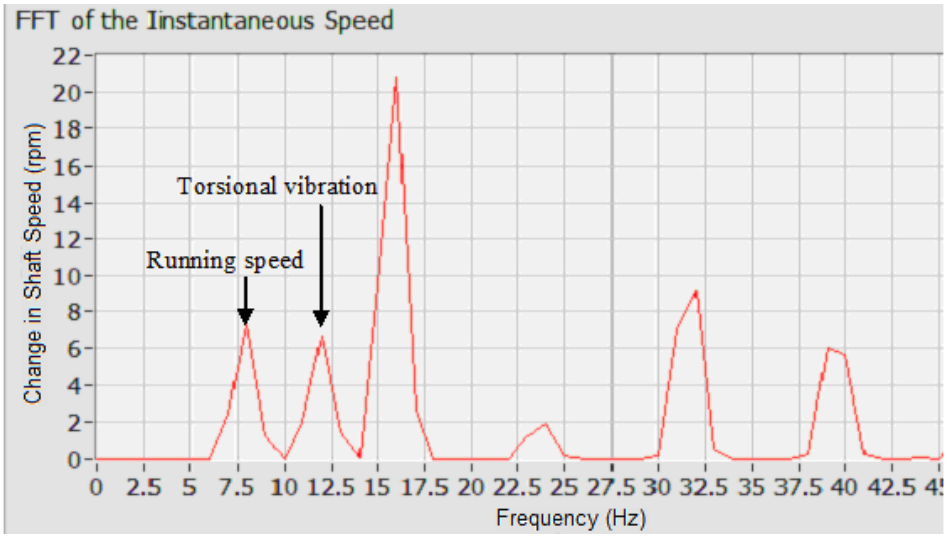

Figure 50: Frequency spectrum of shaft speed using Kar's method at transient speeds.

The torsional vibration was masked within the other frequency components. Again, the source of noise within the signal was attributed to encoder spacing errors along with the calculation algorithm used for determining shaft speed.

These conclusions were further confirmed by viewing the same data set on the LVTorsion measurement system. The signal of the shaft speed generated using this program is shown in Figure 51.

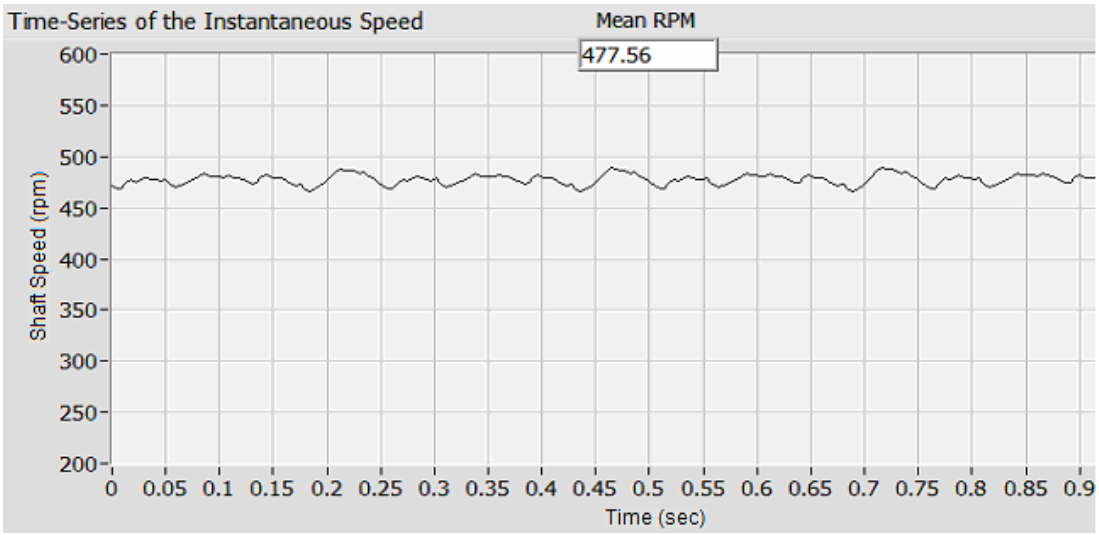

Figure 51: Signal of shaft speed using LVTorsion at transient speeds.

The amount of fluctuating frequency components in the signal was dramatically reduced, which was better demonstrated in the frequency spectrum shown in Figure 52.

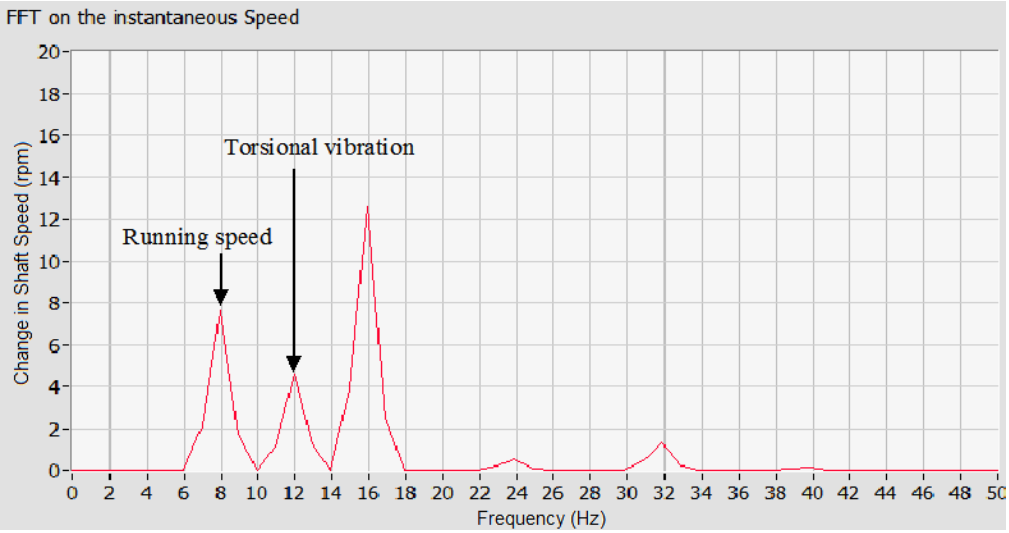

Figure 52: Frequency spectrum of shaft speed using LVTorsion at transient speeds.

A few harmonics of the shaft speed still appear in the spectrum, but most are reduced or eliminated. Changing the speed calculation algorithm dramatically reduced the noise introduced into the system. The leftover harmonics were attributed to the encoder spacing errors demonstrated in the Spacing Error Conformation section.

Sampling Rate

The sampling rate of the data acquisition device was varied in order to determine the maximum relative error in measuring a pulse width. The calculation of the relative error was taken from Equation 14 in the METHODOLOGY section. This equation states that the relative error in measuring the pulse width depends upon the sampling frequency of the DAQ board, the number of encoder segments in one revolution, and the running speed of the rotor. Keeping the rotor speed and number of encoder segments constant, the sampling frequency was varied by the following: 1, 1.5, 2, 3, 5, 10, 20, 50, and 100 kHz. The LVTorsion measurement system was used to measure and process the data. Kar's method was not used during this test because the speed calculation algorithm did not use the pulse width of an encoder segment to determine shaft speed. A carrier signal was generated using the magnetic probe and the taped, metal strip encoder. The Vertical test rig was set to a constant running speed of around 300 rpm and an external torsional excitation frequency of 12 Hz was introduced into the system.

At a 1 kHz sampling rate, the DAQ board missed a pulse every time block; this effect is demonstrated in the shaft speed signal shown in Figure 53.

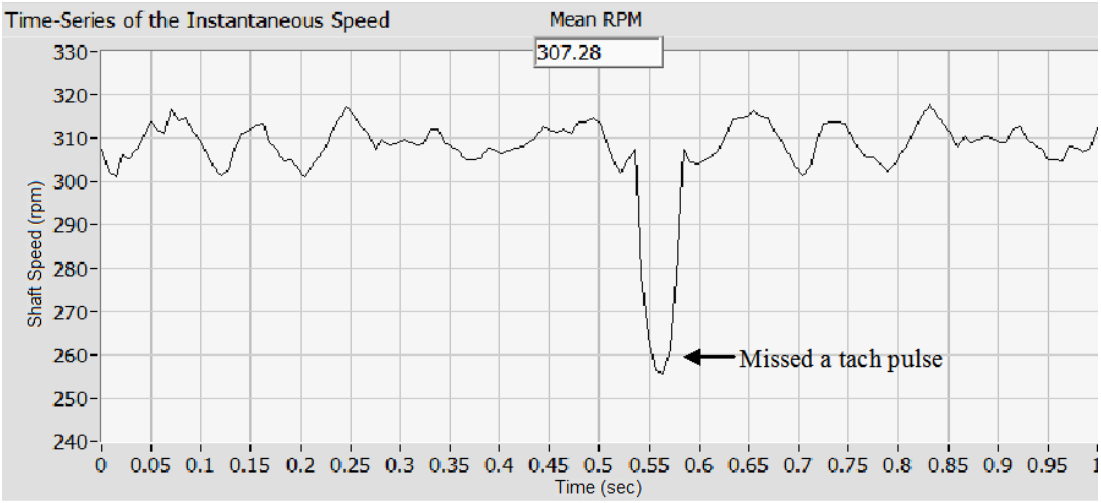

Figure 53: Missed pulse in the shaft speed signal using LVTorsion.

The missed pulse represented itself as an abrupt change in the shaft speed. The abrupt change skewed the frequency spectrum of the shaft speed displayed in Figure 54.

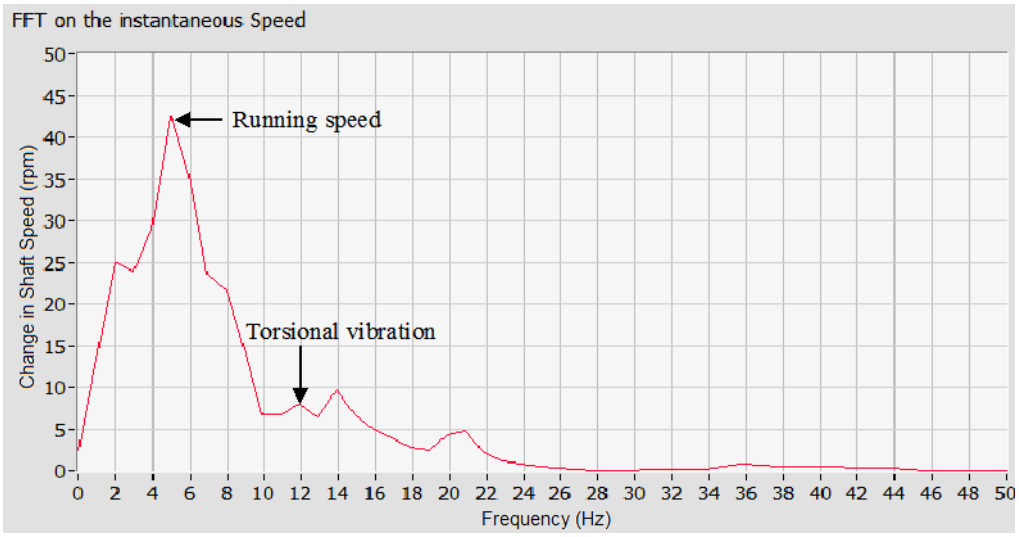

Figure 54: Skewed frequency spectrum as a result of missing a pulse.

This sudden change in the calculated shaft speed almost completely masked the torsional vibration component in the signal. Using the average shaft speed of 307 rpm for a 28

segment encoder with a sampling frequency of 1 kHz, the relative error in measuring the pulse was calculated to be 14%.

It was found that increasing the sampling rate to 1.5 kHz and running the rotor at roughly the same speed eliminated the abrupt changes in shaft speed due to missing pulses. This was apparent in signal of the shaft speed shown in Figure 55.

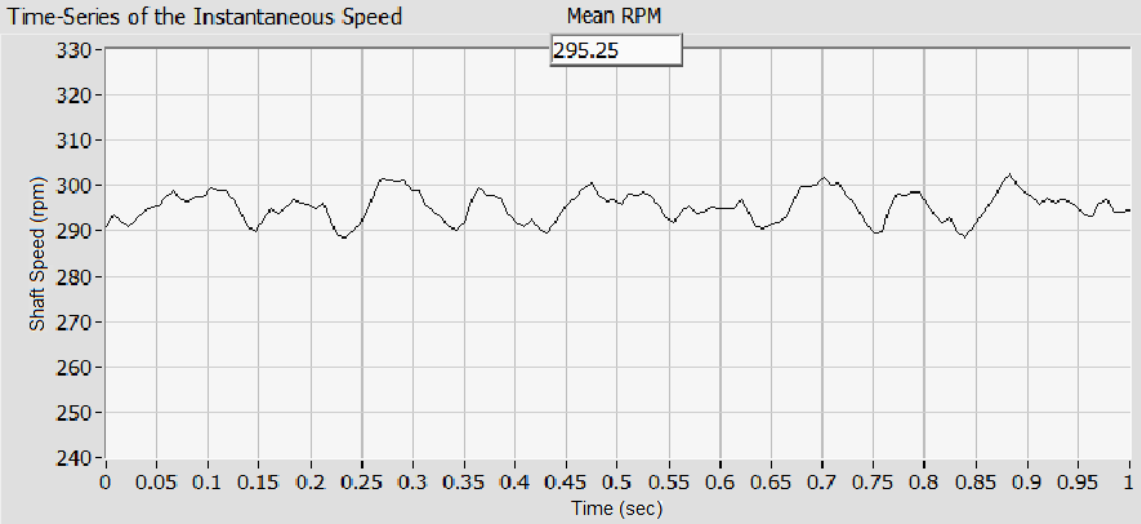

Figure 55: Signal of shaft speed with no missing pulses.

With the sudden drastic change in shaft speed eliminated due to missing pulses, the torsional vibration component was no longer masked in the spectrum as shown in Figure 56.

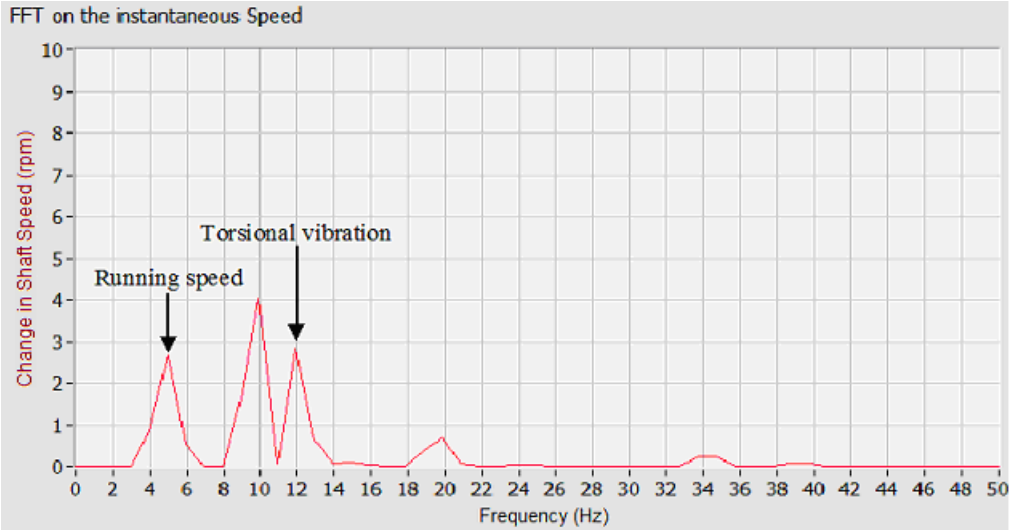

Figure 56: Frequency spectrum of shaft speed with no missing pulses.

Again, the harmonics of shaft speed shown in the frequency spectrum were attributed to encoder spacing error. Using the average speed of 295 rpm for a 28 segment encoder with a 1.5 kHz sampling rate, the relative error in measuring the pulse width of an encoder segment was 9%. It was deduced that anything above a 10% relative error would result in a missed pulse but further testing is needed to confirm this. Increasing the sampling rate past 1.5 kHz did not improve the accuracy in calculating the shaft speed nor did it significantly reduce the noise generated in the signal.

Order Removal

As demonstrated previously, harmonic noise, masking itself as speed fluctuations, make it hard to identify the true fluctuating frequency of shaft speed (torsional vibration). Resampling shaft speed signal into the order domain made it easier to identify the harmonic components in the signal. Knowing their exact locations in the signal, the harmonics were easily removed from the signal.

To demonstrate this method, the Vertical test rig was kept at a constant running speed of around 250 rpm with a constant 12 Hz torsional excitation frequency. A carrier signal was generated using the magnetic probe and taped, metal strip encoder on the top disk of the test rig. The carrier signal was sampled at a rate of 50 kHz with 50k samples in a given time block.

The signal of the shaft speed resampled into the order domain, displayed in Figure 57, showed the same multiple frequency components seen in the shaft speed signals of the previous sections.

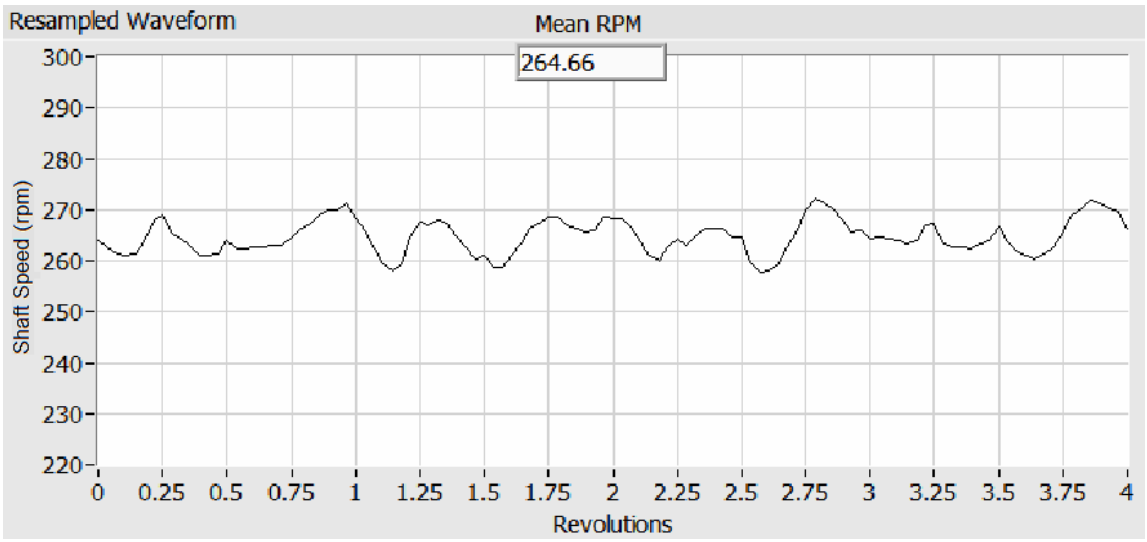

Figure 57: Signal of shaft speed with multiple speed fluctuating frequencies.

When an FFT was applied to this signal, an order spectrum was created, as seen in Figure 58.

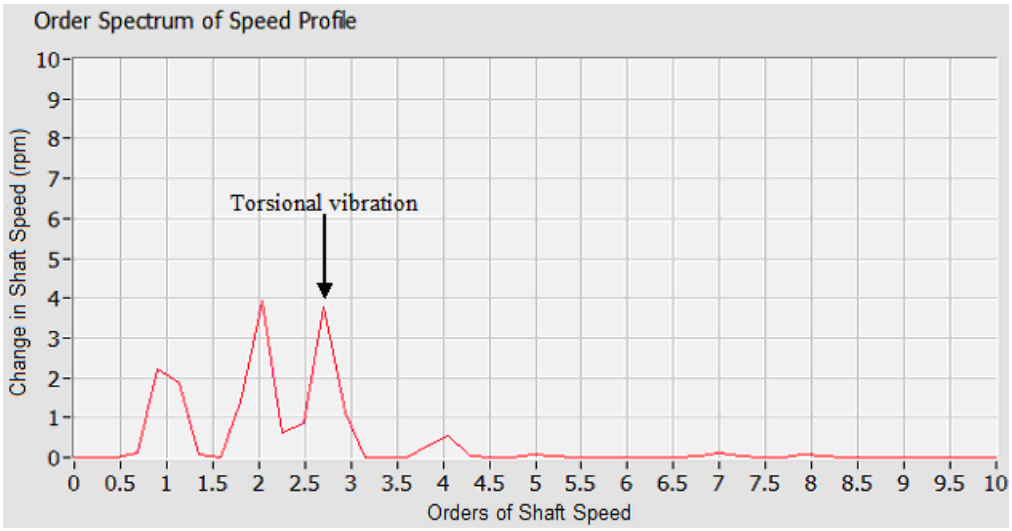

Figure 58: Order spectrum of resampled shaft speed.

The 1st order component represents shaft speed while the 2nd and 4th order components represent 2 and 4 times the running speed respectively. These components were identified and removed from the signal array. The result was an order spectrum, displayed in Figure 59, with all order components removed.

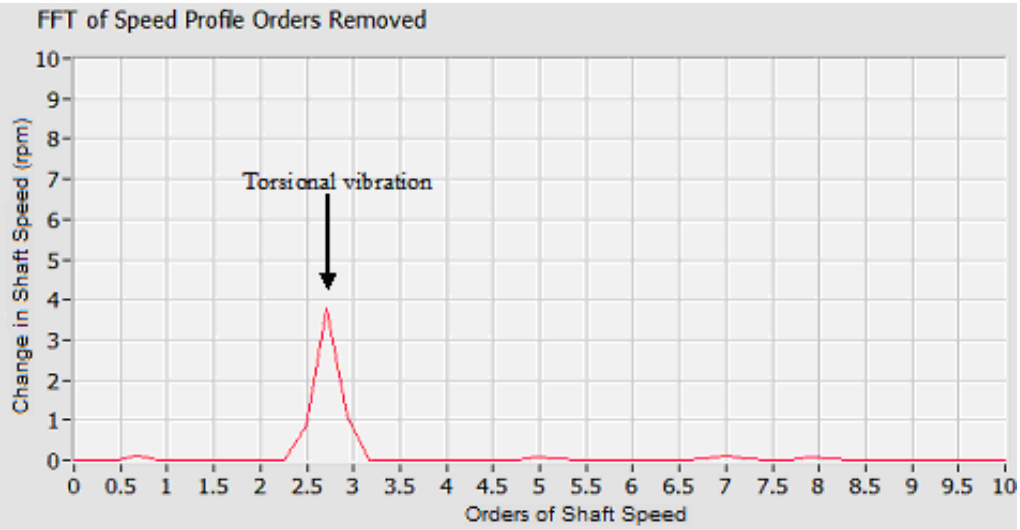

Figure 59: Order spectrum of shaft speed with order components removed.

The only frequency component in the spectrum was torsional vibration. The noise in spectrum was eliminated or reduced significantly. Performing this technique works well when the user knows that the torsional vibration will not occur at harmonics of shaft speed.

To show what would happen if torsional vibration occurred at a harmonic of shaft speed, the speed of the Vertical test rig was increased to 360 rpm or half the torsional natural frequency. The order spectrum, displayed in Figure 60, was generated from the resampled shaft speed.

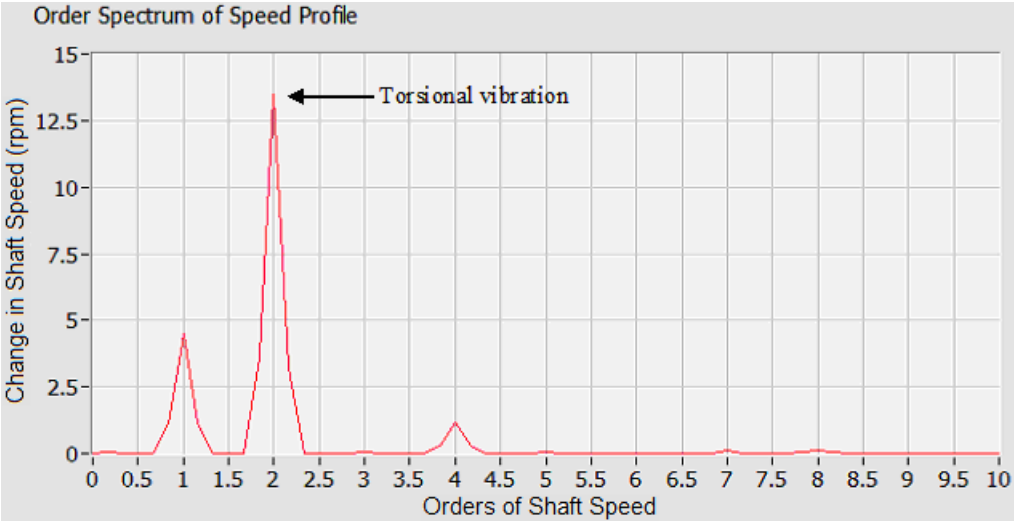

Figure 60: Order spectrum with torsional vibration at 2nd harmonic of shaft speed.

Using the same procedure as before, the order spectrum with harmonic removed resulted in the elimination of the torsional vibration component, seen in Figure 61.

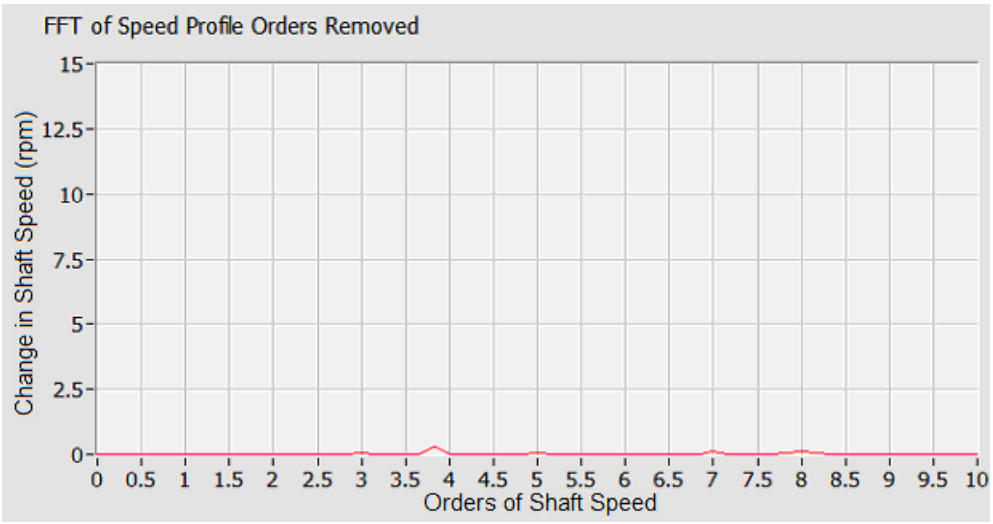

Figure 61: Order spectrum of shaft speed with torsional vibration removed.

Geometric Compensation

It has been proven that a major source of noise in the shaft speed signal is the errors in the spacing of encoder segments. These errors manifest themselves as harmonic components of the shaft speed. When viewed on a frequency spectrum, the noise can mask important frequency components, like torsional vibration, as

demonstrated earlier. One way to reduce this noise is to geometrically compensate the carrier signal to account for the geometric imperfections in the shaft encoder. The algorithm developed in the METHODOLOGY section was used to demonstrate that geometrically imperfect encoders can be used to detect torsional vibration.

Steady-state and transient testing were performed on the Vertical test rig using the geometric compensation algorithm as an analysis tool. A carrier signal was generated using the magnetic probe and the taped, metal strip encoder on the top disk of the test rig. A constant 12 Hz excitation frequency was applied for both tests. The sampling rate of the data acquisition board was 50 kHz with 150k samples in a given time block.

Steady-State Testing

The running speed of the Vertical test rig was held constant at a speed between 250 and 300 rpm. The signal of the uncompensated shaft speed is displayed in Figure 62.

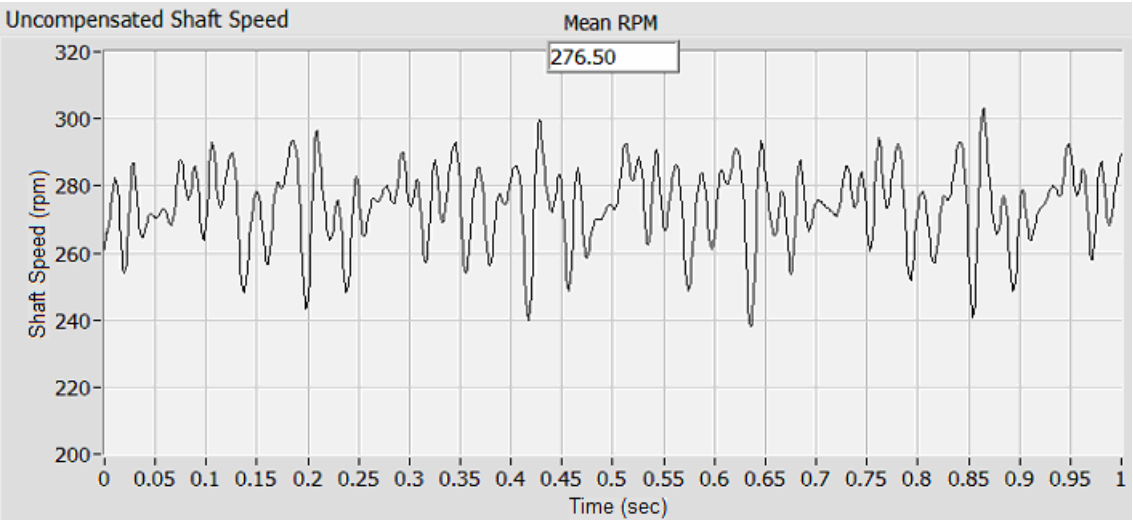

Figure 62: Geometrically uncompensated signal of shaft speed.

A FFT of the shaft speed, displayed in Figure 63, yielded a frequency spectrum with the torsional vibration component amongst the harmonics of the shaft speed.

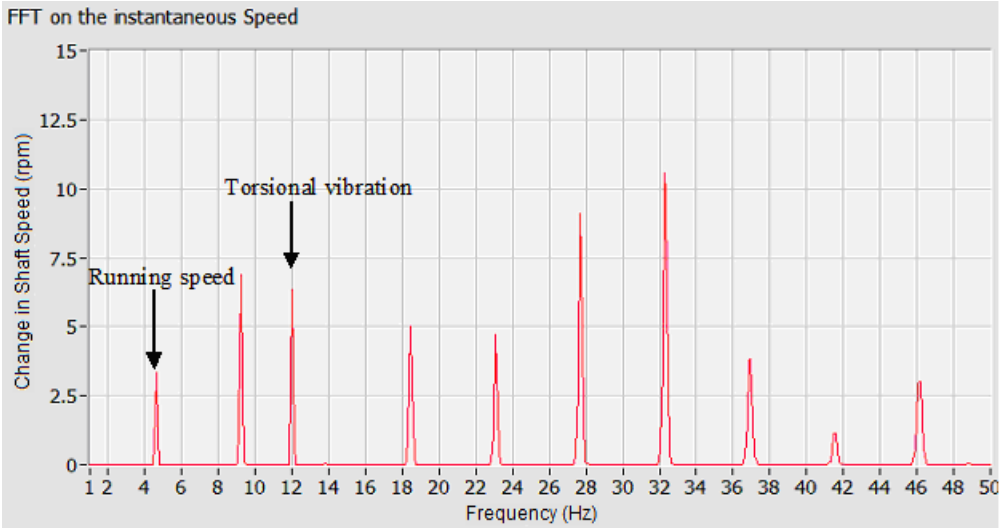

Figure 63: Frequency spectrum of uncompensated shaft speed.

The geometric compensation algorithm produced a signal of the shaft speed, displayed in Figure 64, which removed or reduced much of the noise generated in the signal.

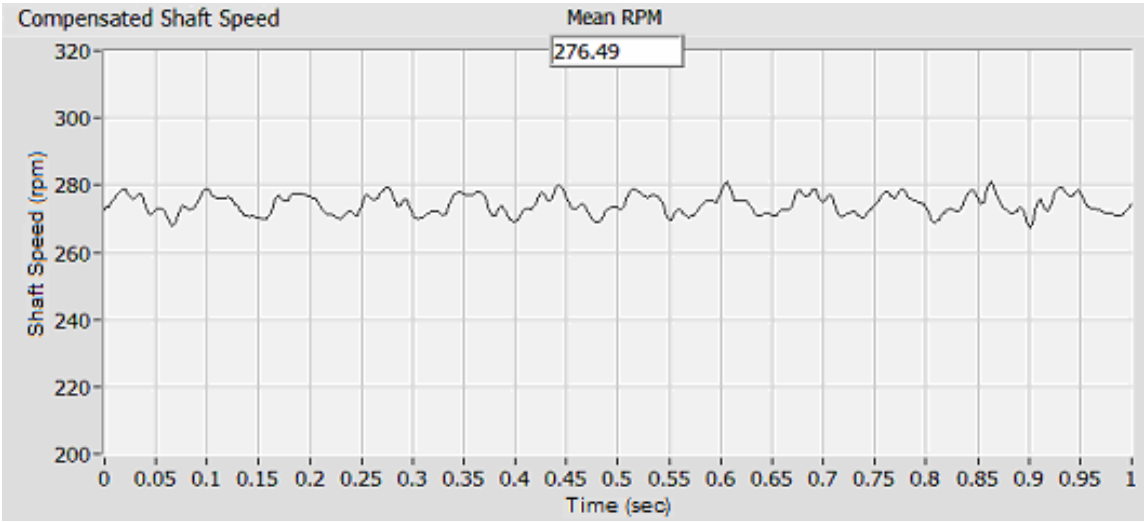

Figure 64: Signal of the geometrically compensated shaft speed at a constant speed.

This signal revealed a strong frequency component similar to the shaft speed signal, displayed in Figure 42, from the high precision machined encoder on the bottom disk of the test rig. The signal in Figure 64 resulted in the frequency spectrum displayed Figure 65.

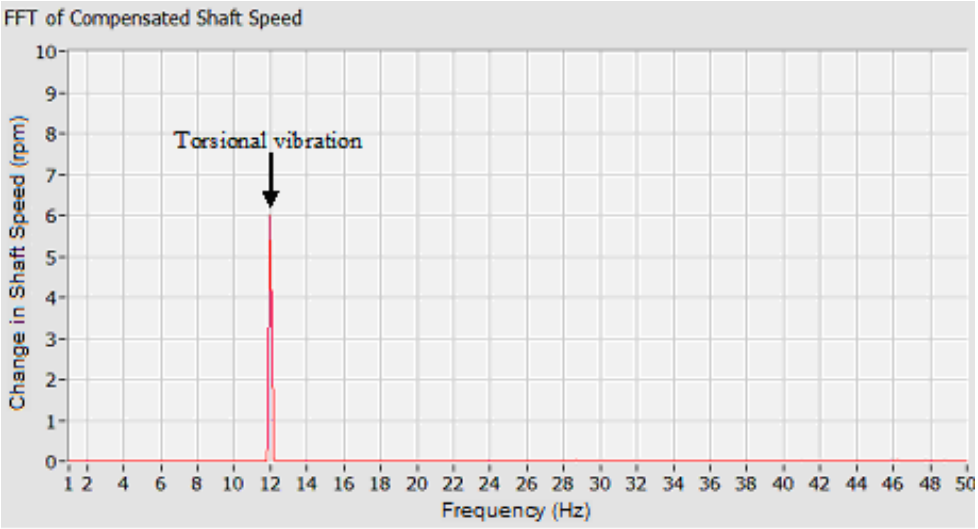

Figure 65: FFT of geometrically compensated shaft speed at a constant speed.

The harmonics of the shaft speed seen in Figure 63 were completely eliminated from the spectrum.

After the initial steady-state testing was performed, the rig was taken up to half the torsional natural frequency or 360 rpm in order to determine if the 12 Hz excitation frequency showed up in the frequency spectrum of the shaft speed. During order removal, the torsional vibration was eliminated from the frequency spectrum when the shaft speed equaled half the torsional natural frequency. Tests showed that the torsional excitation frequency remained in the frequency spectrum of the geometrically compensated shaft speed.

Transient Testing

Transient testing was performed on the Vertical test rig by starting the shaft speed at 200 rpm and ramped up to 500 rpm. The signal of the uncompensated shaft speed is displayed in Figure 66.

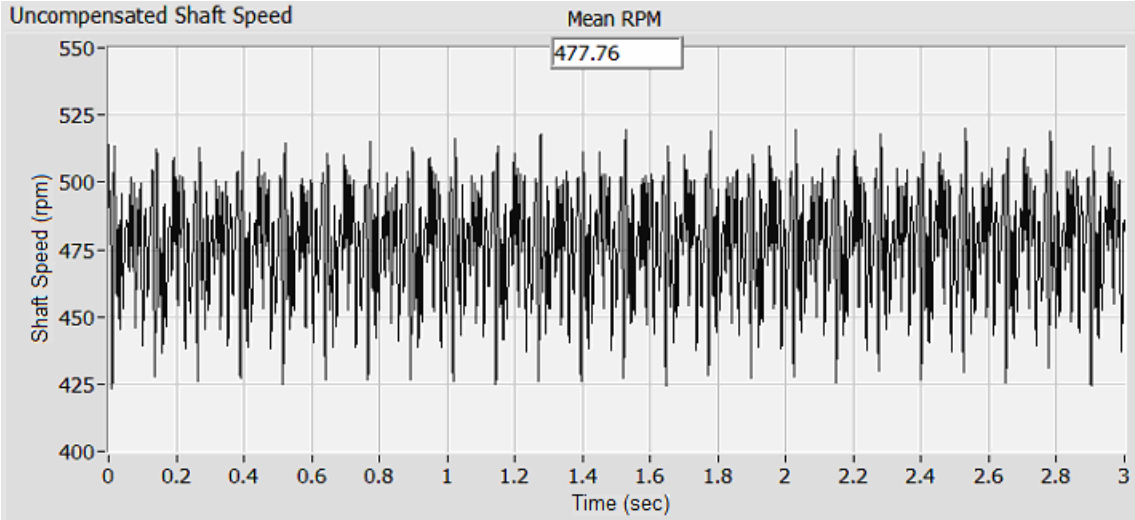

Figure 66: Signal of the uncompensated shaft speed under transient testing.

The frequency spectrum of this signal, seen in Figure 67, yielded a spectrum rich in harmonic frequency components disguising the 12 Hz torsional vibration.

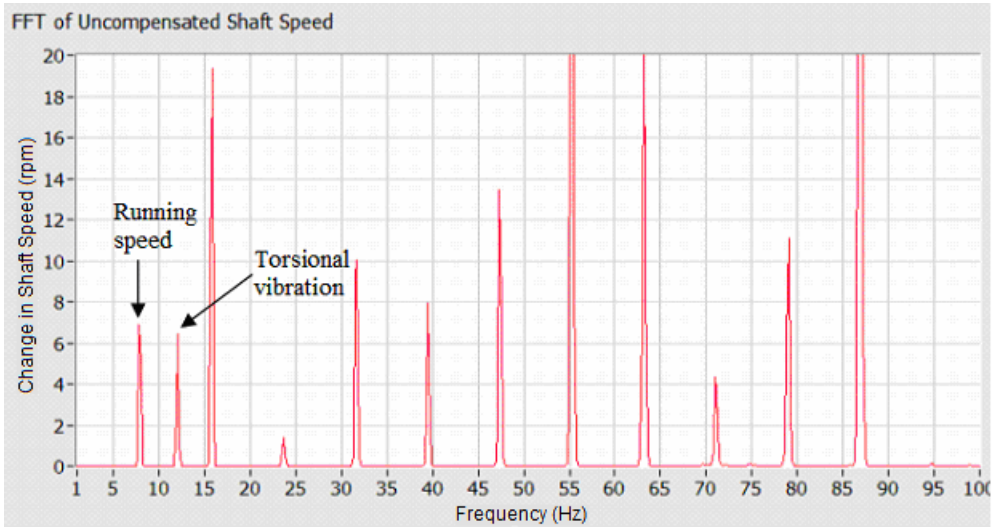

Figure 67: Frequency spectrum of uncompensated shaft speed under transient testing.

The geometric compensation algorithm produced a signal of the shaft speed, displayed in Figure 68, which removed or reduced much of the noise generated in the signal.

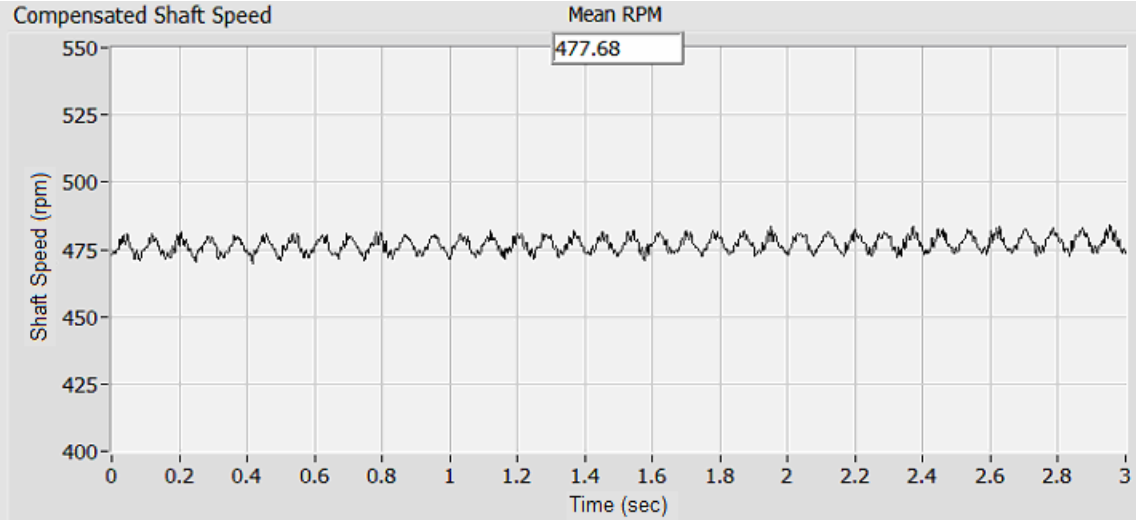

Figure 68: Signal of the geometrically compensated shaft speed at transient speeds.

This signal again revealed a strong frequency component similar to the shaft speed signal, displayed in Figure 64. The signal in Figure 68 resulted in the frequency spectrum displayed Figure 69.

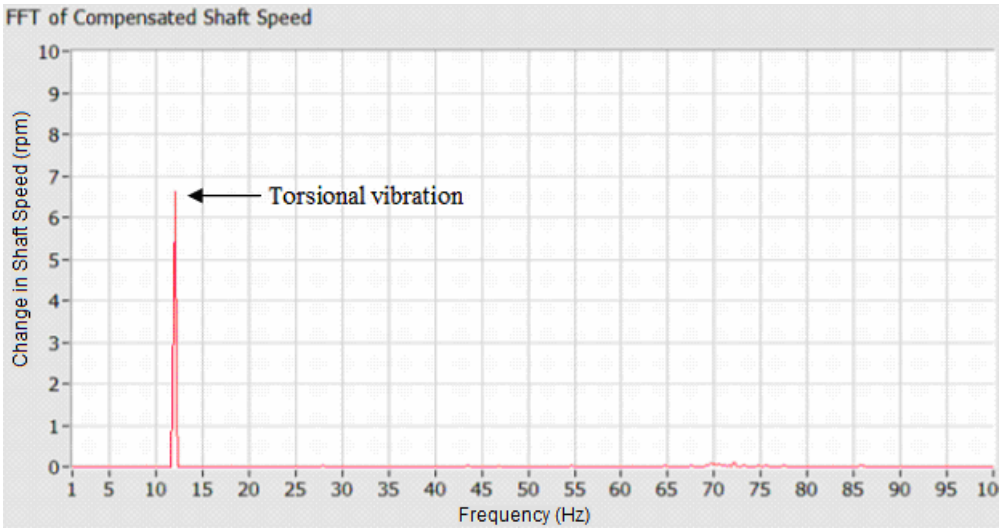

Figure 69: FFT of geometrically compensated shaft speed at transient speeds.

The harmonics of the shaft speed were completely eliminated from the spectrum.

Experimental Verification

Steady-state and transient tests were performed on the T-L test rig in order to verify the results from the Vertical test rig. The test rig was sped up to a speed of 2300 rpm (for the secondary shaft) while a constant 11 Hz excitation was applied to the system. Once the speed of 2300 rpm was reached, steady-state testing with a constant 11 Hz excitation ensued.

The steady-state test results were similar to that of the Vertical test rig. The frequency spectrum of the shaft speed taken from the carrier signal generated at the brake wheel is seen in Figure 70.

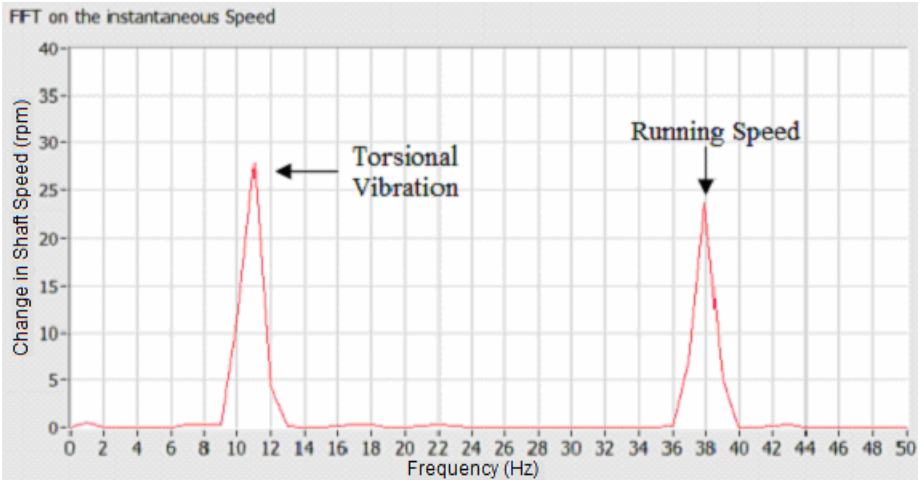

Figure 70: FFT of shaft speed for T-L test rig at constant speed.

The only noise component to show up in the spectrum is at the running speed of the secondary shaft. The order removal method was able to remove the noise at the running speed of the shaft. The order spectrum is displayed in Figure 71.

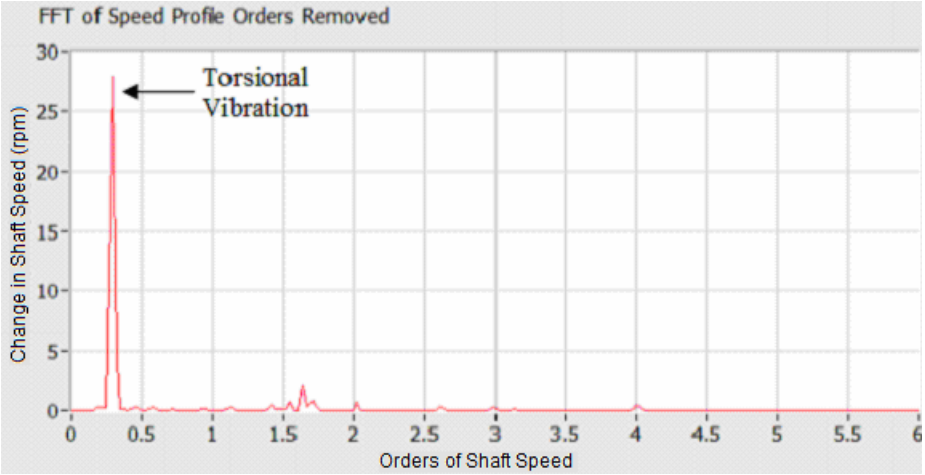

Figure 71: Order spectrum of shaft speed for the T-L test rig at constant speed.

The geometric compensation method was able to remove the noise at the running speed as well. The frequency spectrum of the geometrically compensated shaft speed is displayed in Figure 72.

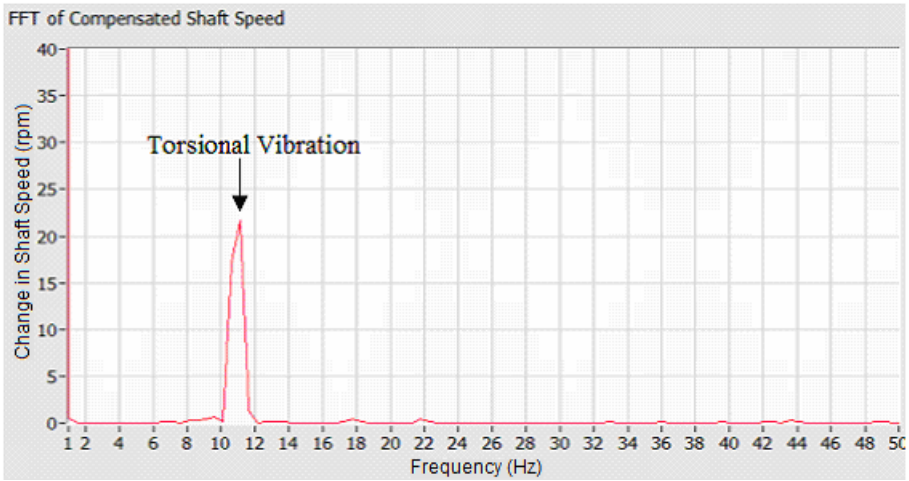

Figure 72: Frequency spectrum of compensated shaft speed for the T-L test rig.

The results of transient testing showed similar results to that of the steady-state testing. The speed calculation algorithm in LVTorsion was able to reduce the noise in the signal of shaft speed to just the noise at the shaft speed. The noise was completely removed from the spectrum using both the order removal and geometric compensation methods.

CHAPTER VI
CONCLUSION

The TIMS measurement technique is a common method used to measure torsional vibration in rotating machinery. Often times, errors are introduced into the system creating noise; such noise can disguise or distort the torsional vibration component in the signal. It was the objective of this thesis to develop and/or test various techniques to reduce the noise introduced into the frequency modulated carrier signal. The following is a list of the techniques developed and/or tested in this thesis:

- created a new algorithm for calculating the angular velocity
- increased the sampling rate of the measurement system
- resampled the shaft speed to an even-angle signal in order to identify and remove harmonic components of shaft speed from the signal.
- developed a method which corrected the algorithm used to calculate the instantaneous speed to account for non-equally spaced encoder segments

All methods were developed and/or tested using the graphical programming software LabVIEW.

Speed Calculation

The calculation method developed by Kar was used as a baseline test to compare the results of changing the algorithm used to calculate the speed of the shaft. In Kar's calculation method, the speed of the shaft was determine by counting the number of pulses in a given time period. A new algorithm was developed that used the pulse width of each encoder segment to calculate the speed of the shaft. This algorithm assumed that the encoder segments were equally spaced.

Steady-state and transient tests showed remarkable ability of the new calculation algorithm in cleaning up most of the noise found in Kar's measurement system. There still remained some noise at the harmonics of shaft speed. It was verified by other testing that these remaining harmonics were due to encoder spacing error. Since the new calculation algorithm assumed equal encoder spacing, any variations in encoder length

appeared as speed fluctuations. Since these error were constant every revolutions, they appeared as harmonics of the shaft speed.

Sampling Rate

The sampling rate of the data acquisition device was varied in order to determine the maximum relative error in measuring a pulse width. Since the new calculation algorithm used the pulse width of each encoder segment to calculate shaft speed, it was important to determine at what frequency to sample the carrier signal. Using the Equation 14 developed by Gomez de Leon, the maximum relative error that could be accepted without missing a pulse was 9%. For the Vertical test, this corresponded to a minimum sampling frequency of 1.5 kHz. Decreasing the relative error (increasing the sampling rate) incrementally to 0.1% showed no appreciable effects in reducing the noise in the signal of the shaft speed. As stated earlier, the remaining noise was due to encoder spacing error and not missing pulses. This helps explain why increasing the sampling rate (after 1.5 kHz) had no effect on reducing the noise.

Order Removal

The leftover noise, after switching to the new speed calculation algorithm, occurred at harmonics of the shaft speed. It was beneficial to resample the signal of the shaft speed to the order domain in order to easily identify the harmonic components with the signal array. Resampling to the order domain was easy to do since the speed at each encoder segment was already being calculated. Once the harmonics of the shaft speed were identified, they were removed from the signal array yielding a frequency spectrum with torsional vibration as the remaining frequency component. This proved to be an effective method in removing the noise attributed to the harmonics of the shaft. The downside to this method was when the torsional vibration occurred at a harmonic of the shaft speed. The result was a frequency spectrum with all frequency components removed, even the torsional vibration. Unless the torsional vibration is certain not to occur at a harmonic of shaft speed, this method runs the risk of removing important frequency components, like torsional vibration.

Geometric Compensation

The majority of the harmonic noise comes from encoder spacing error. One way to remove the noise is to correct the calculation algorithm in order to account for these spacing errors. The geometric compensation algorithm developed in this thesis was able to account for geometric imperfections in the encoder while the rotor was running. Prior measurements of the encoder lengths were not required. Similar correction algorithms have been developed, but most require a once per revolution reference signal in order to identify each encoder segment in the signal; this method required only the carrier signal used for time interval measurements.

Steady-state and transient testing of the geometric compensation technique demonstrated the ability of the technique to eliminate or considerably reduce the harmonic components related to encoder spacing errors. The end result was a clean frequency spectrum with the torsional vibration as the remaining frequency component. The geometric compensation method developed proved to be the most effective of all the techniques in reducing the noise generated in the signal of the shaft speed.

Overall Impact

The TIMS method is an effective technique in measuring torsional vibration. The main reasons for using this method are the non-intrusiveness in acquiring the modulated carrier signal and the relative simplistic algorithm used to calculate the instantaneous speed of the shaft. In order to minimize the noise introduced into the system, most measurement systems require advanced, high precision equipment, such as high frequency counter/timer boards and precision shaft encoders with extremely high tolerances. High precision or advanced usually means high cost. This thesis demonstrated the ability to accurately measure torsional vibration with a geometrically imperfect encoder and at a low sampling rate. With advances in technology and easy-to-use programming software, cheap, in-house measurement systems can easily be developed to measure torsional vibration with a high degree of accuracy.

REFERENCES

[1] J.M. Vance, *Rotordynamics of Turbomachinery*, Wiley, New York, 1988 pp 363-383.

[2] V. Jarvinen, J. Miettinen, Torsional Vibration During the Start-Up of Electric Motor, *Proceedings of SPIE - International Society for Optical Engineering* 4062 (2000) 1888-1893.

[3] K.P. Maynard, M.W. Trethewey, Blade and Shaft Crack Detection Using Torsional Vibration Measurements Part 2: Resampling to Improve Effective Dynamic Range, *Noise & Vibration Worldwide* 32 (2001) 27-30.

[4] R. Kar, J.M. Vance, Investigation of LabVIEW as a Tool for Rotordynamic Measurements and Diagnostics – LVTRC, *Turbomachinery Research Consortium Annual Report* (2005) 47-54.

[5] R.S. French, An Experimental Study of Torsional Vibration Measurement, M.S. Thesis, Department of Mechanical Engineering, Texas A&M University, 1981.

[6] H. Fu, P. Yan, Digital Measurement Method on Rotating Shaft Torsional Vibration, *American Society of Mechanical Engineers*, *Vibration of Rotating Systems* DE-60 (1993) 271-275.

[7] J. Williams, Improved Methods for Digital Measurement of Torsional Vibration, SAE Paper No. 962204, 1996.

[8] F.C. Gomez de Leon, P A. Merono Perez, J L. Aguirre Martinez, Low Cost Procedure for the Measurement of Torsional Vibrations in Rotating Machines, *Proceedings of ISMA* (2002) 1529-1538.

[9] K.P. Maynard, M.W. Trethewey, Blade and Shaft Crack Detection Using Torsional Vibration Measurements Part 1: Feasibility Studies, *Noise & Vibration Worldwide* 31 (2000) 9-15.

[10] B.R. Resor, K.P. Maynard, M.W. Trethewey, Compensation for Encoder Geometryand Shaft Speed Variation in Time Interval Torsional Vibration Measurement, *Journal of Sound and Vibration* 286 (2005) 897-920.

[11] B.R. Resor, Processing and Modeling of Torsional Vibration for Turbine Blade Crack Detection, M.S. Thesis, Department of Mechanical and Nuclear Engineering, The Pennsylvania State University, 2002.

[12] K.Toram, Grinding Medium Oscilliation: Effect on Torsional Vibrations in Tumble Mills, M.S. Thesis, Department of Mechanical Engineering, Texas A&M University, 2005.

[13] A.P. Conkey, Torsional Measurement Using Magnetic Sensors, *Vibration Measurements in Rotating Machinery Project Report*, MEEN 659, Texas A&M University, 1999.

[14] V.N. Rajagopalan, Diagnosing Sub-synchronous Vibrations, M.S. Thesis, Department of Mechanical Engineering, Texas A&M University, 2007.

[15] National Instruments, Data Acquisition Board, Product Services, 11500 N. Mopac Expressway, Austin, TX, USA, 2007.

VITA

Name:	Aaron Michael Schomerus
Address:	Department of Mechanical Engineering, TAMU, College Station, TX, 77843-3123, USA
Education:	B.S., Mechanical Engineering, Texas A&M University, USA, 2005
	B.S., Physics, Sam Houston State University, USA, 2005
	M.S., Mechanical Engineering, Texas A&M University, USA, 2007